Development and Analysis of
Nondestructive Electrokinetic Cartilage Diagnostics

by

Robin Christina Evans

B.S. Mechanical Engineering
Massachusetts Institute of Technology, 1999

SUBMITTED TO THE DEPARTMENT OF MECHANICAL ENGINEERING IN PARTIAL FULFILLMENT OF THE REQUIREMENTS FOR THE DEGREE OF

MASTER OF SCIENCE
AT THE
MASSACHUSETTS INSTITUTE OF TECHNOLOGY

JUNE 2001

Signature of Author: _____
Department of Mechanical Engineering
May 23, 2001

Certified by: _____
Alan J. Grodzinsky
Professor of Electrical, Mechanical, and Bioengineering, M.I.T.

Accepted by: _____
Ain A. Sonin
Chairman, Departmental Committee on Graduate Students

Development and Analysis of Nondestructive Electrokinetic Cartilage Diagnostics

by

Robin C. Evans

Submitted to the Department of Mechanical Engineering
on May 23, 2001 in Partial Fulfillment of the
Requirements for the Degree of Master of Science

ABSTRACT

An electrokinetic surface spectroscopy probe has been developed to take advantage of the bioelectrically coupled properties of articular cartilage. The diagnostic instrument delivers a multiwavelength current to the surface of the tissue and changes in measured impedance are correlated with molecular changes and disease progression. Previous work has demonstrated the probe's ability to detect cartilage degradation in enzymatically-degraded models. In this thesis, the probe is further developed and analyzed. It is assessed in the application of diagnosing engineered tissue repair and surgically induced degradation. The effects of cryopreservation techniques on the impedance measurements are studied. Based on previous limitations in the probe design, a novel impedance probe with permanent electrodes is developed and testing using an enzymatic degradation model. The goal of this thesis is to further develop and analyze electrokinetic spectroscopy as a means to nondestructively diagnose the molecular changes in articular cartilage.

Thesis Supervisor: Alan J. Grodzinsky
Title: Professor
Dept: Department of EECS, Mechanical, and Bioengineering

Acknowledgments

Three cheers for Al, a professor exceptionally dedicated to his students. I learned a new definition of teacher from Al: one who leaves the door to his office open and invites his students to drop by for a meeting "whenever it is good for you". One who is cheerful and motivated at the wee hours of the morning, rolling up his sleeves to work along side you the night before the big DePuy presentation. One who forgives me for backing his car into a fire hydrant (apologies again-aren't you glad I'm going to a country with lots of public transportation?). One who is staying late on a rainy evening to proofread this thesis. One who is thrilled to see our results, excited to answer our questions, pleased to lend out his library and to share his storehouse of knowledge and experience. Thank you for your encouragement and enthusiasm, and thank you for two years of solid academic growth.

Thank you to the lab, for laughs and life lessons learned and excellent cooking and learning to share computers. To Cyndi, avid athlete, collaborator for canine carnage and fellow Switzerland-escapist. Thanks for those times when we'd swivel 'round in our office chairs and discuss the goings-on of the world. And thanks for the company and the histology and even for driving me to the emergency room after that mountain biking trip. Can't wait to visit you in the Alps! To Nora and her multicolored fencing bruises. Thanks for sharing the hugs and the tears. Good luck with fencing—go get those guys! Keep in touch about the heartbreaks and hopes. To Dr. Parth for the late-night therapy sessions. Thank you for your gentle guidance and for helping me to establish a sense of calm in my graduate school experience. To Eliot for encouraging my forray in the the world of bicycling. And electronic circuits. Thank you for answering my calls for help with Dynssap, Dynproc, and demon-possessed computers. To Linda for reminding us about the big world outside the walls of the lab, for introducing me to a humor and compassion uniquely her own. To Gilbert Hung for helping me to burn the midnight oil last year. Thanks for quality conversations and the introduction to henna and Singing Beach. Thank you to UROPs Amanda Yang and Emily Hui. Your assisstance and insights in this project were invaluable and your company and your humor helped preseve my sanity. Best of luck with the rest of your MIT careers! Thank you to Delphine for Death by Chocolate. Yeah! We're done with our theses! Thank you to Jon and John and Alex and Moonsoo and Joonil and Greg for keeping the lab an upbeat and productive place-that is, if you are majoring in video game skills! Thank you guys, for being the expert consulatants and role model researchers. Thank you to HanHwa for keeping this boat afloat!

To my beautiful teammates from MIT Tech Track. Hooray for women's indoor track and San Diego and national qualifiers and sharing long runs and dreams together. Love always. To the gimp squad, a.k.a runners@wind.lcs.mit.edu, a.k.a. the MIT Outing Club for all intents and purposes. Thanks for long runs around the Charles and for getting my butt out in the woods and up on top of some big, big rocks. To my spectacular brother Justin. It was my privledge to finally get to know you this year. Thanks for the prayers and encouragement and for the times we laughed until we cried. Your presence was such a salvation to me this year. Good luck with three more years in Boston. To my kitty Puff for 19 years and counting of feline devotion. To my parents Mike and Becky Evans for

being the best parents and the best friends a kid could have. Thanks for sustaining me with your emails and prayers and long phone calls. Thanks you for keeping my eyes on the big picture and filling my life with your love. And to Aaron McCabe for a crazy journey I wasn't expecting to take. Here's to the future.

Learning continues for a lifetime:

Have you heard that I am a pool shark? A nice gentleman gave the community house a magnificent pool table and we are proving to be a hot bunch. The same mentioned fellow is giving us precise instruction on how to play the best. We are going to beat all the pool halls in town.
Love, Grandma Joan
-my grandmother

"The best thing you've done for me
Is to help me take my life less seriously"
-Indigo Girls

Funny thing about engineering and grades: I think they are inversely related...or at best just completely unrelated.
-Aaron McCabe

My early childhood role models

I'm in the middle of a computer class, so I should probably stop this letter and pay attention!!!!
-my mother

Contents

List of Figures

Chapter 1

Introduction to Articular Cartilage

1.1 Cartilage Function

Articular cartilage is a weight bearing, wear-resistant material found in the synovial joints. Cartilage serves to protect the bone from abrasion and provides cushioning by resisting high tensile, shear and compressive forces and distributing the load to the subchondral bone [35]. It provides joint congruity and maintenance of low stress between opposing bones. The smooth, highly lubricated surface facilitates movement with little friction between articulating surfaces. The surface of cartilage has a coefficient of friction that is several times less than that of ice on ice [51]. Its lack of neural, vascular or lymphatic systems can cause problems for this "wonder material", which otherwise has high compressive strength and low friction coefficient of this When cartilage is injured, pain is not directly sensed, nor can the injury be directly healed without a blood source [35].

1.2 Cartilage Structure

Despite its macroscopically invariant appearance, cartilage is a heterogeneous material whose structural properties depend on the interplay between collagen fibers, proteoglycans, and the fluid phase (figure 1.1). The major macromolecular components of this high modulus connective tissue are the collagen network and the proteoglycan gel in which it is enmeshed. Cartilage is very hydrated, being 80% fluid phase and 20% solid phase. The electrokinetics are a function of the content of tissue, as well as tissue hydration.

1.2.1 Chondrocytes

Chondrocyte cells are enmeshed in the extracellular matrix (ECM). Chondrocytes make up 1-10% of the total dry tissue volume. The cells maintain ECM integrity by mediating the synthesis, secretion, degradation, and turnover of the matrix proteoglycans, glycoproteins, and collagen fibers [40].

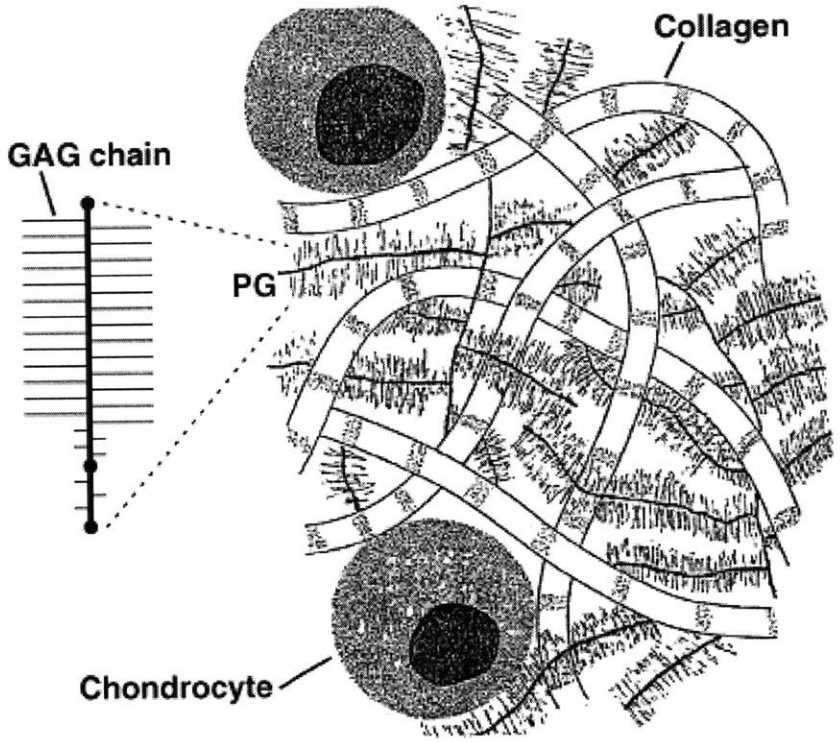

Figure 1.1 A schematic depicting the three main structural components of cartilage: chondrocytes, proteoglycans, and collagen fibers. (Adapted from [15]).

1.2.2 Proteoglycans

The solid matrix is highly negatively charged [28] due to the presence of proteoglycans (PGs) that make up 15-20% of the dry weight. The large aggregating proteoglycan called aggrecan (figure 1.2) has 50-100 glycosaminoglycan (GAG) chains, attached to the core

protein, each GAG consisting of an extended chain of repeating disaccharide units containing approximately one negatively charged sulfate group per disaccharide. Strong electrostatic repulsion exists between the negative charges so that the GAG chains bristle from the protein core [29]. Each aggrecan molecule, in turn, is non-covalently bound to a long hyaluronan GAG chain (figure 1.2), forming a PG aggregate that may contain up to 100 aggrecan PG monomers, together weighing approximately 200 MDa.

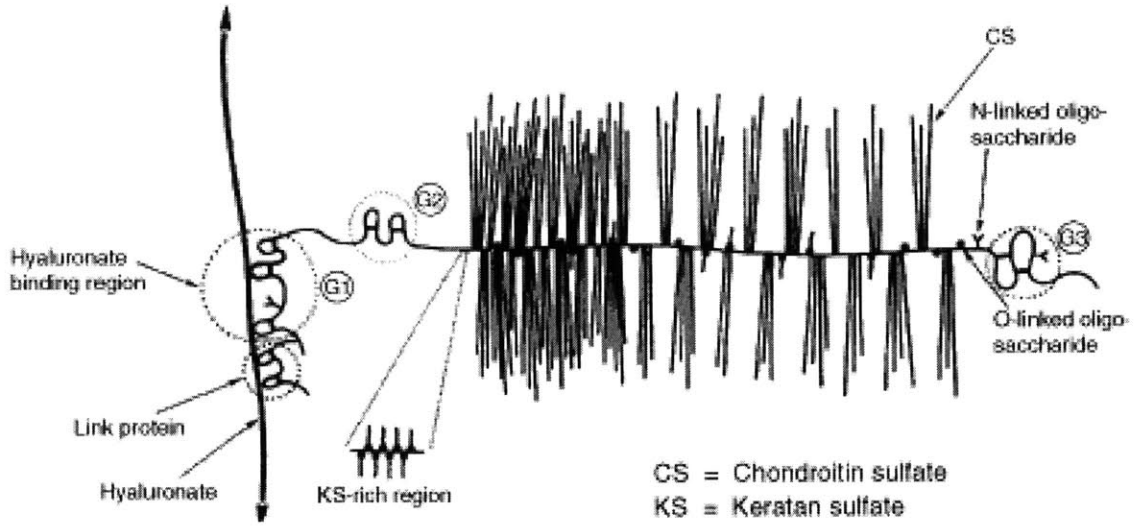

Figure 1.2 Schematic of proteoglycan, showing hyaluron core and sulfated GAG chains (adapted from [15]).

The PGs are important matrix modifiers that create and maintain the water-filled compartments. The high fixed (immobile) charge on these macromolecules attracts counterions. The local high concentration of ions creates an osmotic imbalance and draws water from surrounding areas. The water drawn into the compartments then increases the concentration of macromolecules. The increased molecular concentration may increase reaction rates and promote concentration-dependent reactions [16]. The swelling pressure exerted by the water-filled compartments enables the tissue to resist deformation [2]. Both osmotic swelling and electrostatic repulsion properties of the GAG are essential to the tissue's ability to withstand compressive loads [15].

1.2.3 Collagen

Collagen fibers constitute approximately 50% of the dry weight of articular cartilage [29]. The inextensible three-dimensional lattices of the collagen fibers provide the tissue with its tensile and shear strength. The collagen mesh determines the maximum size of the ECM by trapping and immobilizing the PG molecules. While the water is pulled in by the osmotic swelling pressure of the proteoglycans, the collagen so hinders the expansion and hydration of the tissue that the PG volume is only 20% of its full domain in free solution[2].

1.2.4 Interstitial Fluid

Articular cartilage is roughly 80% water. The interstitial fluid in the tissue carries a light excess of positively charged dissociated ions that maintain electroneutrality at the continuum length scale [28].

1.2.5 Poroelastic Coupling

Cartilage may be modeled as a saturated porous media in which microstructural fluid-solid interactions result in macroscopic coupling between tissue deformation and fluid flow. The electrical, mechanical, and chemical couplings of cartilage tissue are manifested as streaming potentials and streaming currents, electroosmosis, and osmotically induced swelling [28].

1.2.6 Depth-dependent Heterogenity

In adult articular cartilage, the concentration, distribution and macromolecular organization of collagen and PG vary with depth. These into structurally identifiable zones correspond with the distribution of compressive and shearing forces [2].

The superficial zone makes up 5-10% of the total thickness and is characterized by low proteoglycan content and by the collagen fibers that run tangent to the tissue surface. Since the tensile stiffness is proportional to the ratio of collagen and PG concentration, this layer can be seen to have the highest tensile stresses [35]. The properties of the superficial zone allow it to distribute loads evenly over the surface and to resist swelling pressure.

Forty to forty-five percent of the tissue lies in the intermediate layer. Here, one finds an increase in PG concentration, amorphous collagen fibers, and more rounded cells. The next 40-45% of the tissue is designated the deep layer, wherein a high PG content is maintained and the cells are still round. However, the collagen fibers are radially aligned. There is a decline in the tensile stiffness of the deep layer, but it has a greater ability to bear compressive loads [2]. The increase in PG concentration in these layers corresponds with an increase in fixed charge.

At the osteochondral interface is the calcified layer, making up 5-10% of the tissue thickness. In the calcified layer, there is a high concentration of calcium salts and an absence of PG. The collagen fibers are radial and the rounded cells are encased in a calcified cocoon [35]. This layer locks the cartilage to the bone at the chondroosseous junction and functions to convert shear stresses into less damaging compressive forces [2].

1.3 Cartilage Degradation

1.3.1 Acute Trauma

Articular cartilage may be traumatically injured when the knee joint is compressed under heavy load or when angular or shear forces are applied to the surface. The forces may cause softening, fissuring, fragmenting or complete removal of the cartilage and result in pain, swelling, instability and loss of joint mobility [54]. Beyond the initial mechanical

insult, the injurious compression may initiate cell-mediated degradative processes that lead to osteoarthritis (OA). Multiple events such as chondrocyte apoptosis, subchondral microcracks, and joint instability have been linked to the matrix degradation and cell death that are symptomatic of osteoarthritis [34].

1.3.2 Osteoarthritis

A main feature of osteoarthritis is failure of the cartilage's biomechanical properties so that the tissue is unable to withstand high levels of mechanical stress on the joint [49]. Osteoarthritis is the most common form of arthritis, affecting 30-60 million people in the United States. Systemic risk factors include genetics, dietary intake, estrogen use, and bone density, while local biomechanical risk factors include muscle weakness, obesity, and joint laxity [20].

As may be expected from its depth-dependent heterogeneity, cartilage osteoarthritic changes vary with distance from the tissue surface. Surface fibrillation, higher water content, superficial cell necrosis, loss of normal PG orientation, and changes in mineralization characterize OA. There is a net loss of matrix PGs as the chondrocyte-mediated catabolism exceeds replacement by anabolism. This loss unmasks collagen and creates fibrillation at the articular surface. Collagenolytic activity causes cleavage of crosslinks and microfractures of collagen fibrils. The entrapped, underhydrated PGs take up extra water and the tissue swells.

Enzymatic degradation affects both the biomechanical and electromechanical transduction properties of cartilage. When damage occurs in the collagen network, increased tissue swelling results in a lower charge concentration and a possible loss of PG. As PGs are lost, the tissue carries a lower net charge. Once the integrity of the stiff protective outer layer is lost, the underlying tissue is subjected to abnormally high stresses and the degenerative changes extend deeper.

The tissue attempts to repair itself. Osteophyte formation and remodeling at the tidemark are also hallmarks of osteoarthritis. Chondrocytes near the fissures divide and form cell clusters. However, the newly synthesized matrix is ineffective in load bearing [2].

1.4 Intervention and Treatment

In 1743 W. Hunter wrote "ulcerated cartilage is a troublesome thing, once destroyed is not repaired [19]." The avascularity and low cellularity of articular cartilage limits its capacity for repair, and partial thickness defects rarely show signs of healing [13] [31]. While a successful regeneration of cartilage remains elusive, many treatments have been developed to alleviate pain, inhibit further degradation, and stimulate repair. However, valid assessment of these treatments requires nondestructive analysis before, during, and after the therapy, and many require early diagnosis for best results.

1.4.1 Systemic and topical treatments

Mild to moderate osteoarthritic pain may be treated with systemic and topical treatments. Oral medications include non-opiod analgesics and nonsteroidal anti-inflammatory drug (NSAIDS). If the patient does not respond to these medications, more potent but potentially addictive opiod therapy may be applied. Glucosamine and chondroitin supplements have become popular on the consumer market, but there is a lack of a plausible mechanism for therapeutic effect. The NIH is launching the first widespread independent study and results are scheduled to be published in 2004. Topical analgesics are also used to treat mild to moderate pain. Topical creams and gels are most widely prescribed topical treatments for osteoarthritis in the hand or foot [18].

1.4.2 Joint biomechanics alteration

Therapy aimed at altering joint biomechanics may help to decrease the symptoms and progression of osteoarthritis. Studies show that deconditioned muscle, inadequate motion, periarticular stiffness may contribute to signs and symptoms of osteoarthritis [47]. Exercise therapy focuses on (1) range of motion and flexibility exercises, (2) muscle conditioning, and (3) aerobic cardiovascular exercise. Bracing and footwear is another cost-effective and simple alternative to more invasive therapy.

Acupuncture is also gaining acceptance as a nonsurgical treatment. Acupuncture may relieve pain through activation of the neural gate-control system or through the release of neurochemicals. Results from studies are inconclusive, but promising.

1.4.3 Surgical techniques

Surgical treatment of osteoarthritis may be classified as nonbiological or biological treatment. Arthrodesis is a nonbiological treatment in which the affected joints are fused together. While this treatment is usually reserved for small joints, it may also be performed on the hips and knees of small children with unilateral disease [18]. Abrasion arthroplasty and microfracture are techniques that penetrate the subchondral bone in order to promote bleeding and cell infiltration. The repair tissue has been found to fill the defects[32] and to provide symptomatic relief. However, histological analysis has revealed that the repair tissue is composed primarily of fibrous and fibrocartilaginous tissue and hyaline cartilage that lacks normal architecture [45].

Total joint replacement is a widely performed and largely successful surgical treatment. The pain and disability of late-stage osteoarthritis are eliminated and patients return to near-normal function [23][24]. However, the implants have limited durability past 20 years and may limit the activities of more active patients.

The most commonly implemented biological treatments are osteochondral autograft transfers (OATS) and osteochondral allograft reconstructions (OAR). In OATS, a small full thickness defects can be treated by transferring grafts of bone and cartilage from a healthy area in the knee into the defect [54]. The grafts are reportedly taken from "non-functional" areas but that nomenclature is disputed. OAR is a technique of harvesting, testing and preserving bone and articular cartilage from deceased human tissue donors. Grafts up to 4-cm. in diameter have been used to fill femoral condyle surface defects [54]. OAR has been primarily reserved as a limb-sparing procedure for tumor patients and there are considerable infection rates [53].

A variety of matrices, cells, and regulators are being studied for use in tissue engineering. Autologous chondrocyte implantation is currently being engineered on full thickness defects in a weight bearing area of the femoral condyle. A biopsy is obtained arthroscopically from a purportedly "non-functional" area. The cartilage cells are manipulated to replicate matrix, suspended in a liquid medium, and then injected into the defect during a second surgery. While this procedure and many other grafts have shown promise, they still lack the full properties of articular cartilage and have demonstrated only partially integration with host tissue [27], and techniques are currently limited to use on small defects [18]. However, significant symptomatic relief has been provided by the formation of tissue with the cellular, matrix composition, and architecture of fibrocartilage and nonarticular hyaline cartilage [9].

1.4.4 Gene Therapy

A human gene protocol has been developed for rheumatoid arthritis that demonstrates the applicability of orthopedic gene therapy. In this protocol, a gene encoding human interleukin-1 receptor antagonist protein is transferred to the metacarpohalangeal joints. The first patient was treated in July 1996. The experimental data indicates that gene therapy could be beneficial in treating osteoarthritis and cartilage repair. If progress continues smoothly, there could be wide clinical application of gene therapy within 5-10 years [21].

1.5 Diagnosis

This thesis presents the design and analysis of an alternative diagnostic of cartilage degradation. The most prevalently used method of cartilage degradation diagnosis is visual inspection by arthroscopy. This method requires at least a minimal amount of surgical invasion and is only able to detect gross tissue pathology. The physician inspects the surface for roughening, fibrillation, granularity, fissuring, fraying, discoloration, or blistering [10].

Visual inspection is often accompanied by arthroscopic indentation. Physicians palpate the tissue with a blunt indentor and qualitative softness is used an indication of degradation. Dashevsky [10] and Lyrra [29] have developed quantitative indentor probes. However, strain calculations require knowledge of tissue thickness, which must be determined by a second X-ray measurement, and the test provides only mechanical parameters and is not as sensitive as the physiochemical status [40].

Radiography and Magnetic Resonance Imaging have been used to map the three-dimensional geometry and water content of the tissue. These methods are noninvasive and provide significant information, but the details of biochemical degradation are not sufficiently resolvable at the early stages[40]. Blood tests have also shown to reveal signs of osteoarthritis. The partially degraded matrix components diffuse out of the cartilage and into the synovial fluid. The components then enter the lymphatics and eventually reach the circulation [2].

Biochemical analysis may be done on tissue biopsies. GAG assays are performed with dimethylmethylene blue (DMMB) dye to assess PG content, hydroxyproline assays test for collagen cleavage, and the tissue may be lyophilized in order to calculate its water content. While, there is no correlation among these properties in non-OA tissue, the PG content decreases and the water loss increases as OA progresses. However, these are relative compositional changes and no absolute correlation has been established [39]. Moreover, the tissue must be damaged to obtain biopsies.

1.6 Electromechanical Surface Spectroscopy

An electromechanical surface spectroscopy probe has been developed to take advantage of the coupled properties of cartilage tissue. In electromechanical surface spectroscopy, a sinusoidal current applied to surface of another medium and the resultant response is measured. When a sinusoidal current density is applied to the cartilage tissue surface via an excitation electrode array, the fixed negative charge in the matrix is pulled toward the positive electrodes and the intratissue fluid is displaced toward the negative electrode (figure 1.3) [14]. The fluid convection of the counterions separating from the oppositely charged matrix molecules creates a streaming potential. Due to the macroscopic coupling between tissue deformation and fluid flow, the flow produces a mechanical perturbation, which may be measured with a surface stress sensor and recorded as the *current-generated stress* [5]. The voltage drop across the electrodes may also be measured and the ratio of the voltage and the applied current may be recorded as the *impedance*.

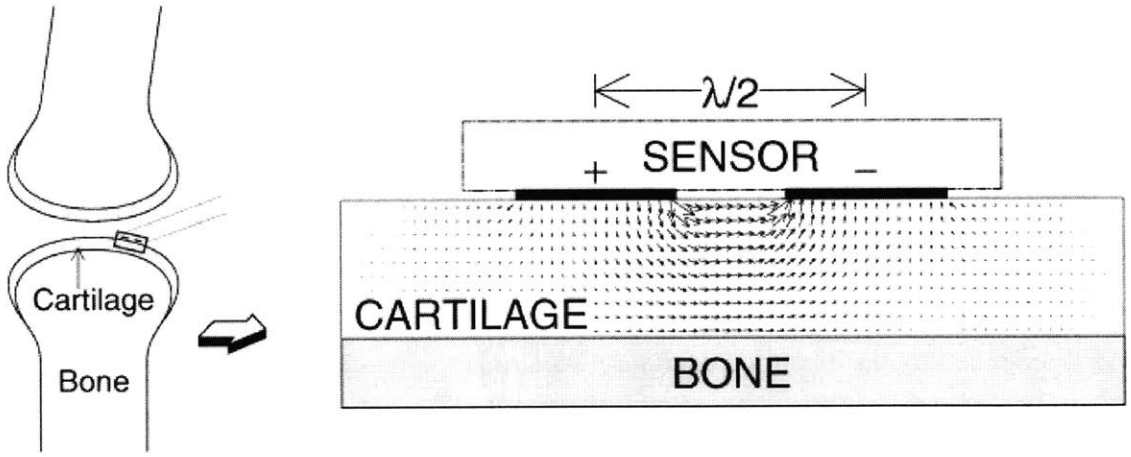

Figure 1.3 Electromechanical surface spectroscopy. Probe with excitation electrodes array mounted on cartilage. The arrows show the intra-tissue current density profile [40] (Adapted from S. Berkenblit[6])

1.6.1 Development

Frank [11] developed a uniaxial configuration for cartilage spectroscopy in which current was applied via electrodes on opposite ends of the excised cartilage plug. Sachs [41] later demonstrated in a mathematical model that two silver electrodes placed on the same surface side of cartilage could induce a measurable mechanical response when current was applied. This technique had the advantage of being potentially nondestructive.

Salant [43] and Berkenblit [6] subsequently designed a hand-held spectroscopic probe to produce excitations on the surface of the cartilage tissue with an interdigitated array of electrodes. The probe could measure the bulk material properties of dielectric materials [55] such as cartilage by applying a spatially and temporally periodic sinusoidal signal and evoking a simultaneous electrical or mechanical response that could be measured at the same surface. The benefits of dielectric spectroscopy in cartilage diagnostics are that it is nondestructive and that varying the imposed spatial wavelength may test different depths of tissue. One may test for spatial inhomogeneities and detect molecular level changes.

1.6.2 Variable wavelength imaging

The variable wavelength imaging was first tested in the current-generated stress modality. A probe was constructed with four independently addressable electrodes. The wavelength was determined by the electrode excitation pattern at the tissue surface. The characteristic depth of penetration of the imposed current density is approximately 1/3 the spatial wavelength of the current [5] so that a short wavelength could assay the superficial region of the tissue, while long wavelength would assay the full thickness. In this manner, one could image depth-dependent focal lesions.

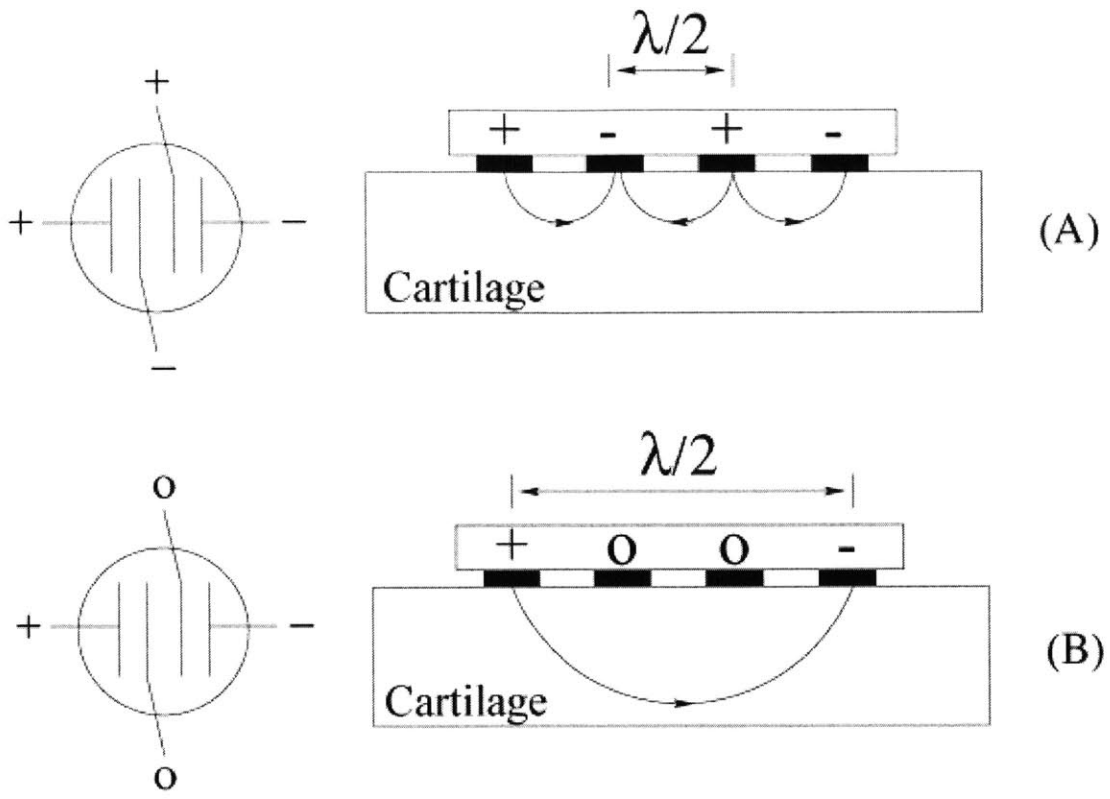

Figure 1.4 Short (A) and long (B) wavelength penetration (Adapted from S. Treppo [50]).

Calf cartilage was subjected to trypsin digestion as a model of aggrecan degradation. A diffusion chamber was designed to allow the enzyme to contact tissue only at the surface so that a longer exposure time would result in deeper penetration. The probe was used to measure the short and long wavelength stress response of disks before and after trypsin. In the normal tissue, the short wavelength response was approximately half of the long wavelength response, while after a 2-hour trypsin treatment, the short wavelength response decreased significantly compared to long wavelength [5]. This *in vitro* model system provided controlled PG loss from tissue, and the significant decrease in the measured stress in the enzymatically degraded tissue compared to controls confirmed the sensitivity of current generated stress to monitor molecular level degradation and showed ability of the probe for spatial imaging [4].

1.6.3 Collagen degradation model: current generated stress and impedance

The probe was shown to be able to produce two simultaneously measured outputs to detect controlled degradation *in vitro* as induced by using matrix metalloproteinases (MMPs) [6]. MMPs have an important role in the degradation and turnover of ECM molecules such as type II collagen and aggrecan. They regulate both normal remodeling and disease progression [44]. Two MMPs in particular, MMP-1 and MMP-13, are found in higher levels in osteoarthritis tissue [7][45]. The spatial and temporal changes in molecular activity caused by MMPs result in functional changes in mechanical and electrical changes. This study measured molecular level changes in collagen-proteoglycan matrix using both current-generated stress and impedance.

Bovine osteochondral cores were placed enzymatically degraded in MMPs for up to 24 hours. They were placed in diffusion chambers that allowed only surface penetration. The bathing medium assayed extent of matrix degradation. An 800 μm disk removed from top and placed in contact with surface probe. A current density of mA/cm was applied to the surface of the tissue over a frequency range of 0.025-1.0 Hz. The tissue was also stained with monoclonal antibody 9a4 to localize damage to collagen molecules.

It was found that the most intense collagen damage occurred at surface. While the MMP-1 had degraded down to 0.8 mm by 24 hours, the MMP-13 had only penetrated 50 μm. The release of PG increased with time. The current generated stress was analyzed as a short-wavelength to long wavelength stress response ratio (SR). The SR decreased significantly in MMP-1 by 24 hours at 0.025 Hz, but there was no significant difference for buffer alone or MMP-13. It was seen that the minimum wavelength $\lambda = 3.23$ insufficient to measure change in MMP-13 using CGS. However, the impedance modality was sensitive to changes even at extreme superficial layer. There was a significant increase in impedance at all frequencies in the long wavelength configuration for both MMP-1 and MMP-13. The most significant increase occurred at greater frequencies. The increase was likely due to decreasing PG content and increased swelling at constant PG.

1.6.4 Impedance detection of trypsin-induced matrix degradation

The first impedance experiments with the handheld probe were conducted on bovine osteochondral cores were exposed to trypsin for 4 hours, with surface-only digestion. Controls were divvied up as either 0-hour trypsin, 24-hour trypsin, or 0, 4, or 24 hours in buffer. The digestion buffer was collected and assayed for PG degradation. The top 1mm of each core was placed in contact with probe at increasing strain at 0, 10, 20, 30, 40, and 50%. Only the two inner electrodes were used to apply a current density of 1 mA/cm2 at 1, 10, 100, and 1000 Hz. Biochemical assays were used to test for hydration and GAG content.

The trypsin treatment significantly reduced GAG content The GAG loss increased with digestion time and was concomitant with a significant increase in hydration. As the applied current frequency increased, the impedance magnitude decreased. As the strain on the tissue increased, there was a monotonic decrease in impedance for all frequencies. The difference in impedance between the control and treated tissue was frequency-dependent. At 1 Hz, the enzymatically-treated tissue had a higher impedance than controls, while at 1000 Hz, control tissue had higher impedance than enzymatically-treated tissue.

This result was due to the frequency-dependence of the electrode-electrolyte interfacial impedance. The interfacial impedance may be modeled as a conductance and resistance in series, so that its magnitude was much greater as low frequencies such as 1 Hz than at higher frequencies such as 1000 Hz. The impedance measurements have since been conducted at frequencies of at least 100 Hz to minimize the affect of the interfacial impedance.

The electric charge distribution at the electrode-electrolyte interface results in a capacitance and a leakage resistance across the charge double-layer, so that the interface can be equated to a resistance R_d and a capacitance C_d in parallel (figure 1.5). The

resistance and impedance may then be lumped into an interface impedance. Subsequent measurements have also been normalized to the impedance of the probe in a buffer solution in order to account for variations in interface conditions.

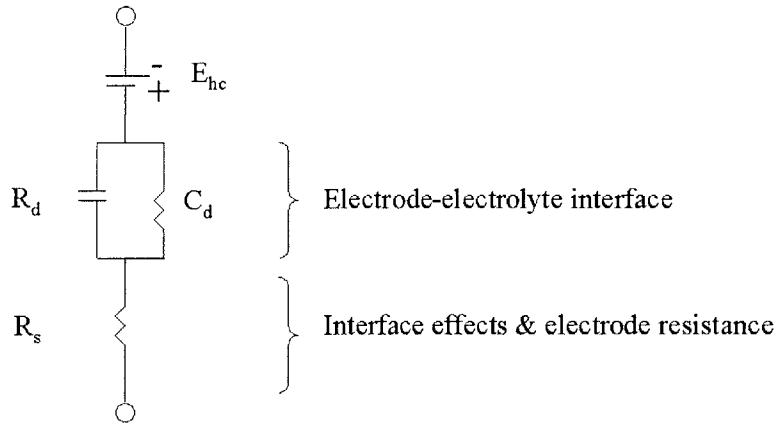

E_{hc} = half-cell potential
R_d = leakage resistance across the double-layer of charge
C_d = capacitance across double-layer
R_s = saline/PBE resistance

Figure 1.5. Equivalent circuit for a biopotential electrode in contact with an electrolyte, composed of the half-cell potential, the impedance associated with the electrode-electrolyte interface and polarization effects, and the series resistance associated with interface effects and due to resistance in the electrolyte. Adapted from Neuman [33].

1.7 Outline of Results

This thesis reports several studies performed using an impedance probe to detect the bioelectric properties of articular cartilage. Attention is paid to molecular-level changes in the matrix that are induced by human osteoarthritis, autologous graft treatment, and enzymatic degradation models. Because of cartilage's heterogeneous composition, the measurements are analyzed for depth-dependent changes that yield more sensitive and detailed information about the state of the tissue. The impedance measurement system is therefore assessed for feasibility as a diagnostic for detection of early-stage degradation and of the efficacy of subsequent repair treatments.

Chapter 2 presents the impedance probe system, including changes made since previous publications. In chapter 3 the impedance probe is used *in situ* to assess its ability to diagnose graft repair and to detect secondary degradation from the graft therapy. The need to test samples that had previously been frozen was the motivation for the study in chapter 4, in which the effects of cryopreservation on the impedance of cartilage samples is measured. Finally, in chapter 5, a novel impedance probe with permanent electrodes is developed and tested with an enzymatic tissue degradation model. The thesis will be summarized in chapter 6.

The results of a study on the measurement and comparison of the degradation of intact human patellar joint surfaces at different stages of osteoarthritis are compiled in appendix A. Appendix B contains information about a new design for a handheld spectroscopic probe using current-generated stress (CGS) to diagnose the electrokinetic state of the tissue, and in appendix C is the summary of business plan for the CGS probe.

Chapter 2

Electrokinetic Surface Probe in Impedance Modality

2.1 System setup

2.1.1 Probe construction

A hand-held impedance probe with disposable electrode sensors was used in the experiments in this thesis, unless otherwise specified. The modular design was composed of disposable sensors mounted onto a cylindrical body with three main parts: the inner core, the insulating sheath, and the outer stainless steel body (figure 2.1).

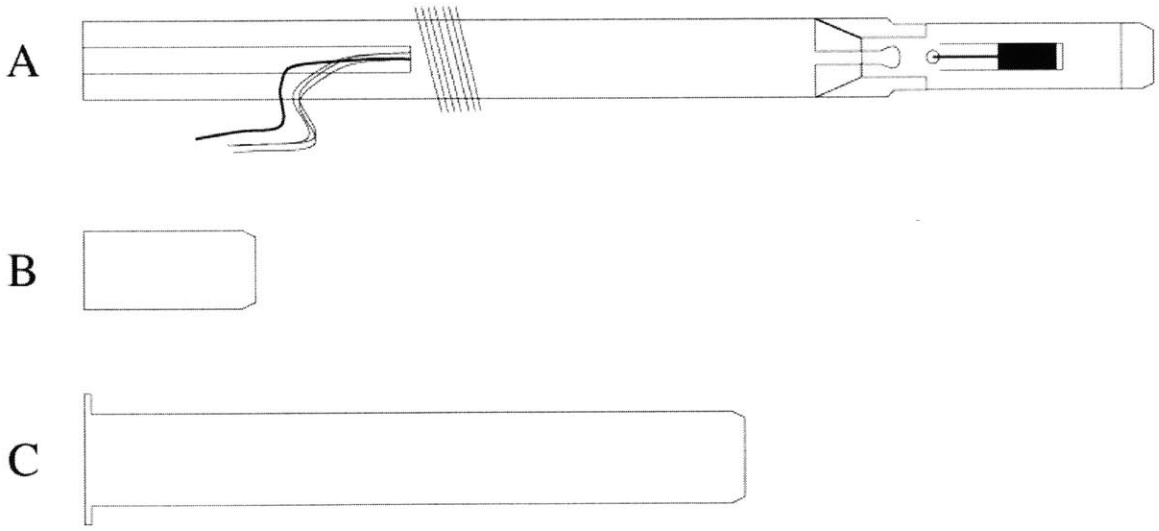

Figure 2.1 The probe body was composed of three main parts: the inner core, the insulating sheath, and the outer stainless steel body. (Adapted from E. Quan [37])

A thin disposable laminated electrode structure (ES) was used to apply the current via silver excitation electrodes that were photofabricated on an insulating metallized Mylar layer. A backing plate was bonded to the metallized Mylar side of the ES (figure 2.2). The backing plate aligned the ES with a machined recess on the tip of the probe to ensure

that the electrodes were mounted to a flat surface and were properly oriented to the electrical connections.

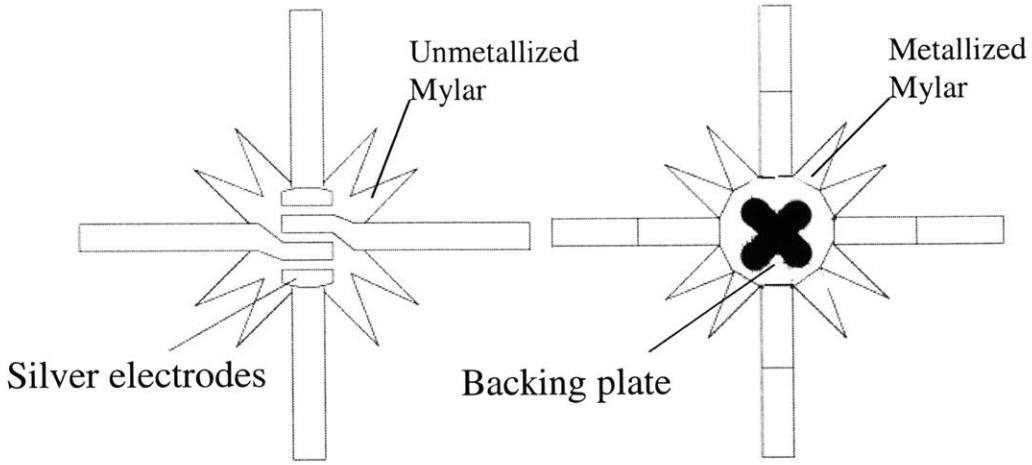

Figure 2.2 Electrode sensor (ES) front and back, showing silver electrodes and backing plate. [Modified from E. Quan [37]].

The ES was fixed on the tip of a cylindrical torlon core that housed the four individually insulated wires carrying the driving current to embedded copper contacts. A thin cylindrical sheath of delrin was pressed over the ES to stabilize the contact between the silver electrode arms and the copper contacts. The sheath also electrically insulated the ES and the electrical connections on the probe core.

The delrin core sits on a stainless steel body and this inner core subassembly was clamped into a stainless steel outer tube with a screw to create a sealed environment. The steel shell acted as a conductive ground plane that sent extraneous signals to ground. Silicon adhesive was applied after mounting to provide additional sealing at the ES-sheath and sheath-outer tube interfaces.

2.1.2 Sensor Fabrication

Electrode sensor construction

The electrode sensors (ES) were fabricated as previously reported by Treppo [50] and Quan [37]. A 25.4 μm-thick silver foil (Johnson Matthey, Ward Hill, MA) was cut to

11mm^2 and a 25.4 μm Mylar polyester film (MADICO, Woburn, MA) was cut to 10 mm^2 square. The Mylar was metallized one side with aluminum. The silver film was cut to the size which would allow it to have electrical connection with the brass contacts, and the Mylar film was cut to the size which would allow it to be electrically grounded to the inner core to provide shielding. The surface of the silver was abraded with a slurry powder to remove surface impurities in preparation for the photofabrication and chloridation. A two-part urethane epoxy (Tycel 7000/7200, Lord Corp., Erie, PA), thinned with methyl ethyl ketone, was used to bond the Mylar and silver. Only a thin layer of epoxy was desired, to maintain flexibility. The unmetalized side of the Mylar was bonded to the silver so that the metallized side was grounded through contact with the stainless steel rim of the inner core.

Photofabrication

The electrodes were created through photofabrication. To optimize photofabrication, the ES was cleaned in a mild detergent (Alconox, Alconox Inc, New York, NY), and dipped in 15% nitric acid so the surface would be slightly acidic. The ES was thoroughly rinsed in deionized water (DI) and was convection baked to remove moisture.

An even layer of photoresist polymer (KPR Photoresist, KTI Chemicals, Sunnyvale, CA) was pipetted onto each sensor. The resist allowed to dry for 20-30 minutes and then dried in convection over for another 10 minutes. The ESs with the dried resist layer were placed in registered masks. The masks were placed between two glass plates in exposure apparatus and exposed under UV light for 15 minutes. The unmasked areas were crosslinked under UV light so that they were resistant to chemical etching. The masks and glass plates were wiped carefully to remove dust that could prevent polymer crosslinking and cause holes and cracks in the electrodes. The sensors were then rinsed in a xylene-based developer (KPR Developer, Alphametals, Jersey City, NJ) for a total of a minute, washed in warm tap water and DI water to wash off uncrosslinked photoresist, and blotted dry.

Etching, Stripping, Cutting

Etching dissolved the silver not protected by the crosslinked photoresist. The sensor was blotted dry and mounted in a Teflon holder that exposed the center of the silver in a well. A 55% ferric nitrate etchant was pipetted into the well and agitated for 12-14 minutes. The etchant was replaced approximately every two minutes to maintain potency. The etching was complete when the silver around the electrode was gone and the Mylar beneath was exposed. The ES was removed and rinsed with DI water.

A toluene-soaked (Mallinckradt, Paris, KY) cotton swab was used to rub off the nonconductive photoresist on the electrodes. The ES was washed again in a gentle cleanser and rinsed in DI water. A sharp scalpel was used to cut the 0.4" wide silver arms and the star-shaped folding pattern.

Assembly

A 0.33-mm backing plate was affixed to the back of the sensor to align the silver electrodes with the probe body electrical contacts and keep the sensors flush against the probe tip. The backing plate rested in the recess when sensor was placed on the probe. A cotton swab was used to hold the sensor in place while the delrin sheath was placed over the head of the probe. The electrical connection between the silver arms of the sensor and the copper tabs on the side of the probe was checked with a multimeter. When the connection was established, a thin layer of silicon adhesive sealant (Superflex Clear RTV Silicone, Loctite Corporation, Rocky Hill, CT) was applied to the sheath-sensor interface. The sheath was then completely pressed over the probe head and the excess sealant was wiped from the electrodes.

The stainless steel outer body was placed over the subassembly and after rechecking for electrical connections, another thin layer of silicone was applied to the stainless steel-sheath interface. All of the parts of the probe were pressed together by tightening a neural nut. The connections were checked again and the sealant was allowed to dry overnight.

Chloridation

The chloridation step plated the silver electrodes with a silver/silver chloride layer by means of a closed-loop electrolytic cell. Applying a silver chloride deposit alters the stabilization of the electrode potential and also the impedance between the electrode and the bathing electrolyte [12].

The magnitude of the interface impedance depends on the thickness of the chloride deposit. Chloridation reduces the interface impedance by creatin an increased surface area. Too much chloride deposit, however, will increase the resistance to current flow. It has been empirically determined that the optimal silver chloridation for minimal electrode-electrolyte impedance occurs at 1000mAs/cm^2 [12]. For the four 1.59mm^2 electrode configuration on the ES, the current was set to 71 μA and the reaction was run for 15 minutes.

The electrodes were abraded with sandpaper to prevent nonuniform deposit of chloride. The probe tip was then suspended in a chamber with unbuffered 0.1M NaCl pH 4.0. The four electrodes were connected to the positive terminal of a Hewlett Packard 6214A DC power supply in series with a Keithley ammeter and a 10 kohm resister, which approximated a constant-current source. A platinum electrode was suspended in the bath and connected to the negative terminal (figure 2.3). The electrodes were shorted together while the current was then turned on and adjusted to the desired value. When the chloriding was to begin, the short was opened and the current passed through the chloriding bath to create a redox reaction that deposited chloride ions onto the silver electrode.

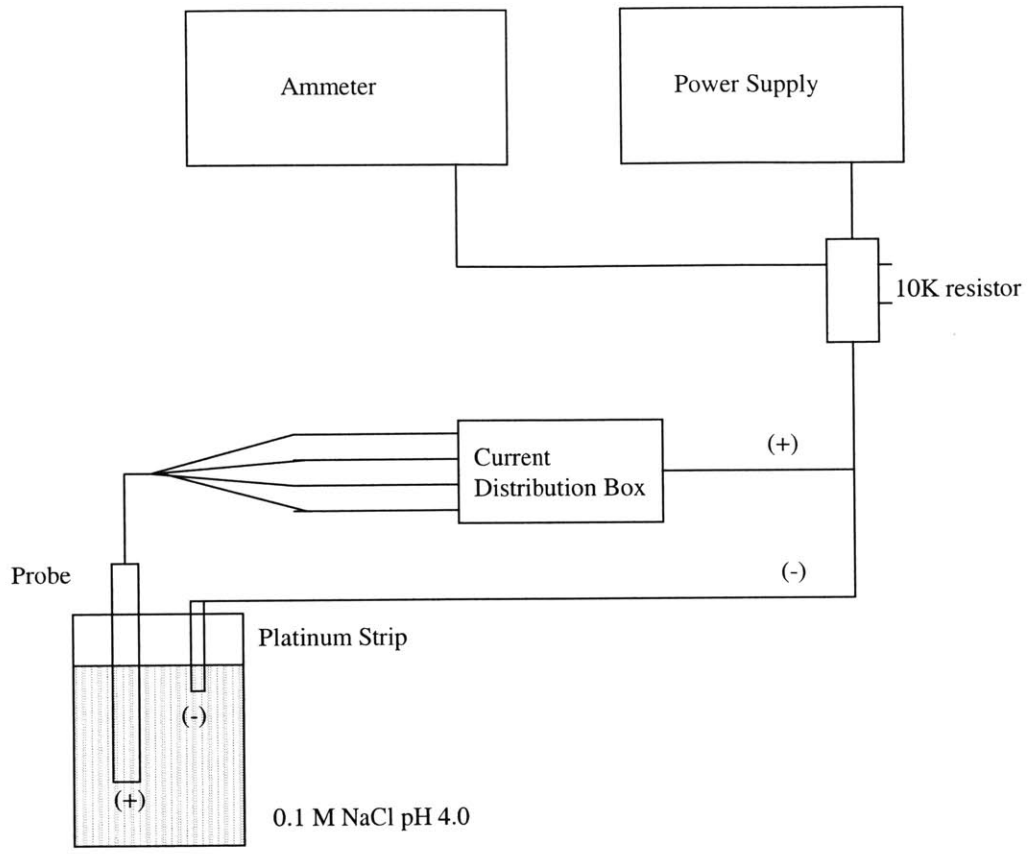

Figure 2.3 Schematic of chloridation setup. A redox reaction plates the silver electrodes with chloride ions.

2.1.3 Hardware setup

The current parameters are determined by computer settings. The operator designates amplitude, frequency, wavelength, and repetitions. This information is sent to the current source and to the electrometer. The current source is powered by an external power supply and delivers the specified current amplitude and frequency to the current distribution box, and provides the electrometer with the measured voltage drop across the electrodes. The current source also communicates with the electrometer for auto-drift correction. The electrometer also sends waveform information to the current distribution box. The current distribution box directs the polarity of the four excitation wires that drive the sensor electrodes (figure 2.4).

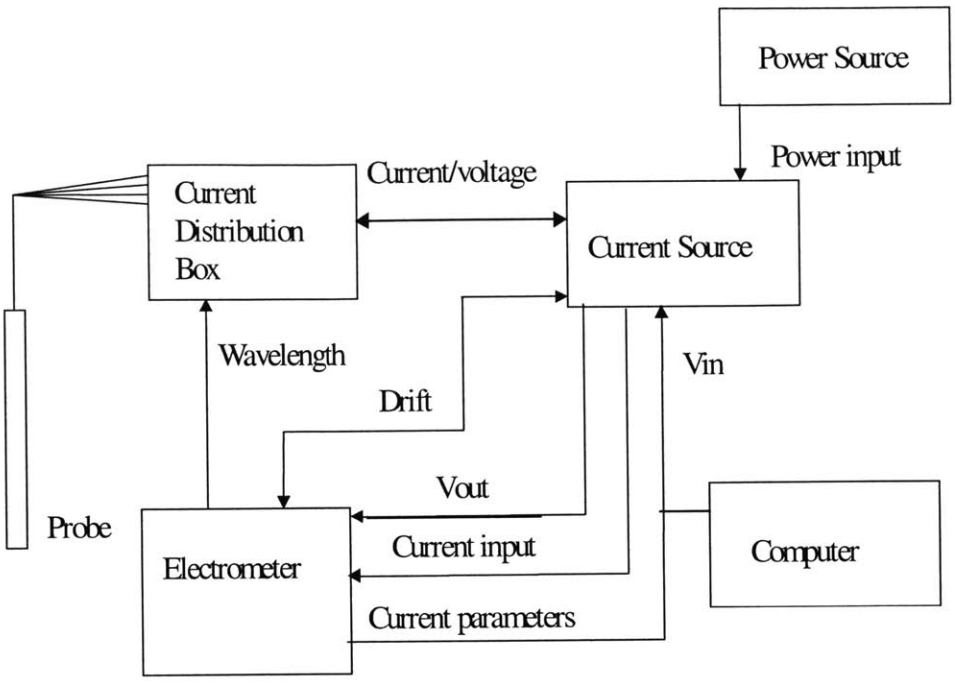

Figure 2.4 External electronics

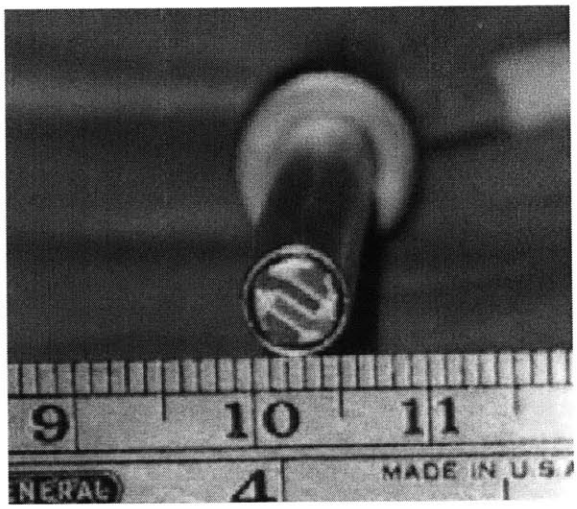

Figure 2.5. Fabricated, assembled, and chlorided impedance probe. Adapted from E. Quan.

Figure 3.1 The impedance probe being used *in situ* to measure femoral patellar groove graft tissue impedance at the Veteran's Association Hospital in Roxbury, MA.

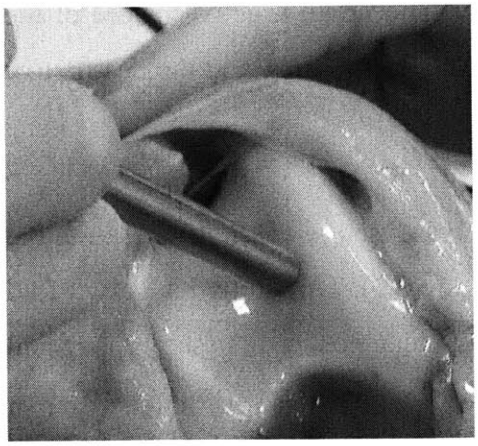

Figure 3.2 Close-up of the impedance probe being used *in situ.*

Chapter 3

Quantitative Impedance Analysis of Canine Articular Cartilage Tissue Following Graft Implantation

3.1 Introduction

The aim of this study was to test the probe for potential *in vivo* measurement of molecular changes in articular cartilage after chondrocyte transplantation. Cultured autologous implantation is one of the most widespread treatments of chondral defects at this time. The efficacy of this treatment is the subject of much debate and studies suggest that the procedure may also have a degenerative effect on the surrounding tissue [27]. However, *in situ* testing of the effects of the transplant on the donor site and the transplant site has been limited by available technology. The quantitative and nondestructive nature of the probe renders it an improvement over qualitative mechanical probing and the destructive biopsies required for biochemical assays.

The electromechanical surface spectroscopy probe was used *in situ* to measure the electrokinetic properties of canine cartilage tissue (Figure 3.1). This study had a two-fold objective. The first was to assess the probe device as a diagnostic of tissue repair, and canine repair graft tissue on the femoral patellar groove impedance (Figure 3.2) was compared with histological, mechanical, and electromechanical measurements. Secondly, we wished to further assess the ability of the probe as a diagnostic of tissue degeneration. We measured the degenerative effects of the surgical procedure on untreated, articulating tissue and compared the measured impedance with tissue hydration and GAG content.

3.2 Analysis of Femoral Patellar Graft Tissue

3.2.1 Methods

Surgical Procedure

This animal experiment was approved by the Brockton/West Roxbury VA Animal Care Committee and the surgical procedure was performed using a protocol previously reported [8]. Chondrocytes were harvested from the trochlear ridges of six mature hound dogs. The harvest involved the removal of a strip of tissue approximately 20-25 mm long and 3-5 mm wide down to the tidemark. The cells were cultured in monolayer up to third passage and seeded in N-3- (3-dimethylaminopropyl)-N-ethyl-carbodiimide (EDAC) Cross-linked type II collagen matrices (Chondrocell, Geistlich Biomaterials, Wolhusen, Switzerland), the pore characteristics of which have been previously reported [26]. The matrices were implanted in 4-mm surgically constructed defects in the contralateral joint. The right knee joints of the animals were immobilized for ten days, after which ambulation appeared normal. The animals were sacrificed 15 weeks after implantation (Figure 3.4).

Impedance Measurements

At necropsy, impedance measurements were taken by placing the electrokinetic probe on the surface of the opened right knee joint. The impedance measurements were made using a 4.5-diameter sensor on the tip of the probe. In this study, the electrodes were configured so that the current penetration depth was 0.7mm as shown in Figure 3.3.

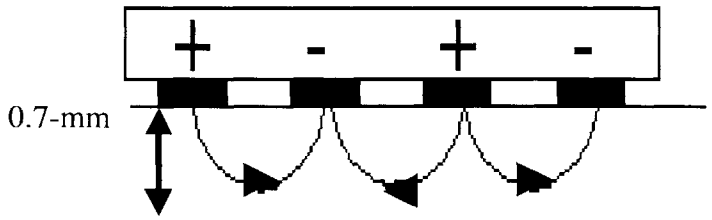

Figure 3.3 The electrode polarities were configured so that the current penetration was approximately 0.7-mm.

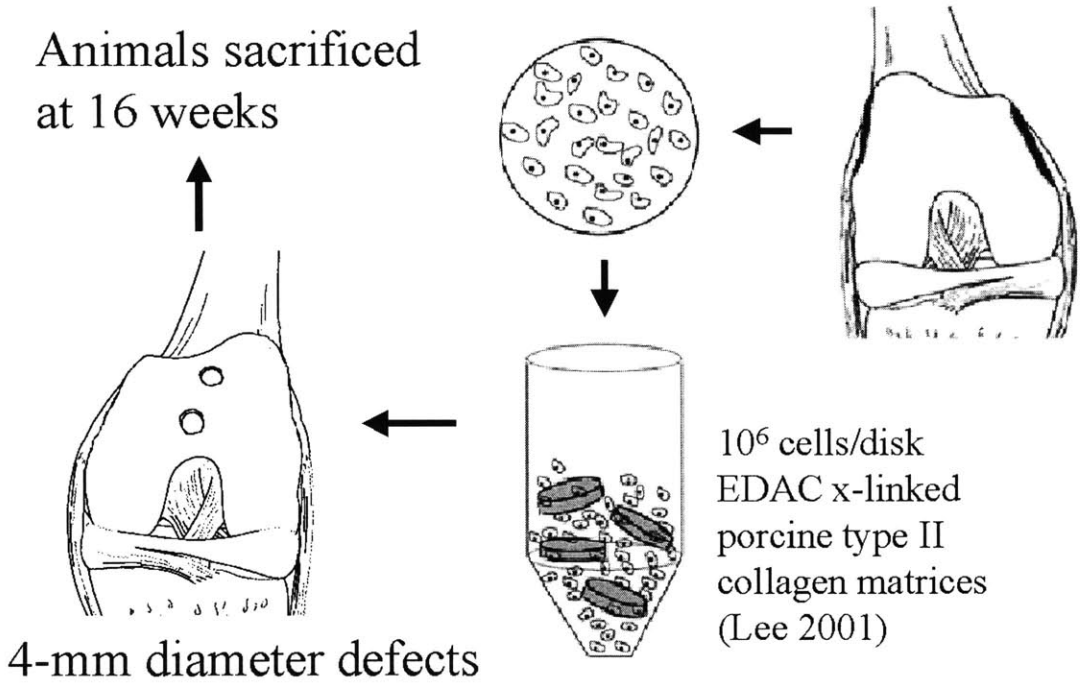

Figure 3.4 Surgical procedure for the harvesting chondrocytes from the trochlear grooves on the left knee, seeding the chondrocytes in collagen matrices, and implanting the graft tissue into surgically constructed defects.

In the short wavelength configuration, for a current density of J = 1.0 mA/cm2, the total driving current amplitude was 31.8 μA. The impedance was then calculated as the ratio of the measured voltage drop across the electrodes to the applied current.

The probe was placed on the surface of the femoral patellar tissue with a 50kPa offset stress. Measurements were taken on the proximal defect, the distal defect, and at an adjacent normal tissue site as outlined in Figure 3.5. Before and after each measurement on the tissue, a measurement was taken in 0.15M PBS to determine the impedance of the interface and the buffer used to hydrate the tissue during the procedure.

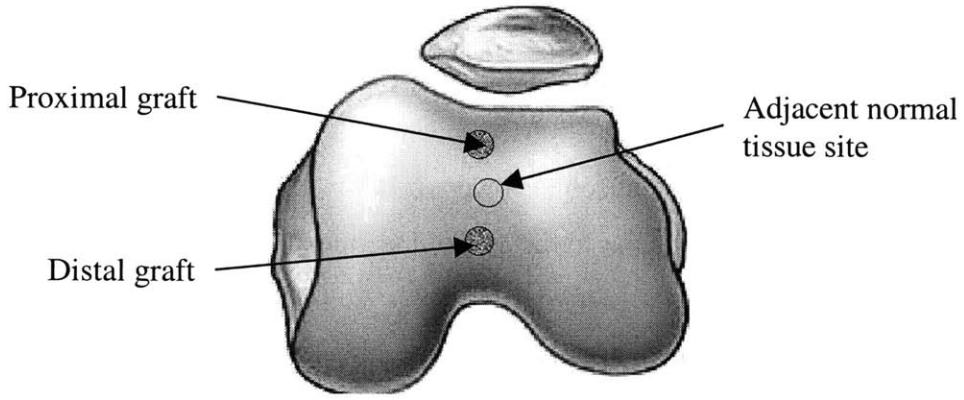

Figure 3.5 The impedance probe was used to take reading at the proximal and distal graft sites, and at an adjacent normal tissue site.

The impedance was measured on the tissue surface as well as in the buffer solution for reference. The buffer measurement impedances were taken immediately before and after each tissue measurement, averaged together, and the tissue impedance was then normalized to this averaged buffer impedance. The measurements were then grouped by site (proximal, distal, and adjacent normal), and a student t-test was applied to compare each site group. Significance was determined at $p<0.05$ and $p< 0.01$. Impedance data is presented below as mean +/- standard error. The averages were taken for each of the three frequencies measured (100 Hz, 300 Hz, 1000Hz).

Specimen Procurement and Allocation for Testing

The right patellar grooves containing the defects were removed using a coping saw and wrapped in saline-soaked gauze. The proximal graft was removed for histology, using a safarin O stain, while the distal graft was reserved for mechanical testing and streaming potential.

Mechanical and Electromechanical Testing

The specimens were prepared for mechanical testing as described previously (Lee Harvest). The distal graft sites were cored with a 9.5-mm bit and the underlying one was mounted in self-curing polymethylmethacrylate (PMMA; Quickmount, Fulton Metallurgical Products Corp., Saxonburg, PA). The specimens were placed in a chamber with five rotational/translational degrees of freedom. The chamber was clamped into the lower jaw of a Dynastat mechanical spectrometer (IMASS, Hingham, MA) and a 1-mm diameter cylindrical, plane-ended PMMA indentor with an Ag/AgCl electrode was mounted in the upper jaw. The specimens were positioned so that the testing site on the cartilage surface was perpendicular to the axis of the indentor.

Three sequential step loads were applied to the specimen, reaching approximately 10, 15, 20% strain, and equilibrium loads were recorded. Sinusoidal displacements with amplitudes corresponding to approximately 1% strain and with six different frequencies ranging from 1.0 Hz to 0.005 Hz were superimposed on the 15% static strain, and the resulting dynamic loads and streaming potentials were recorded. The free-swell thickness was measured using a needle-ramp method [17] and used to calculate the actual static and dynamic strain amplitudes.

Histology

The proximal graft from each subject was reserved for histological staining. A 9.5-mm osteochondral core was drilled around the graft site. The cores were placed in 10% formalin immediately after specimen procurement. After fixation, the plugs were decalcified in 15% EDTA for at least twenty-eight days. They were then dehydrated and

embedded in parafin. Seven-micrometer sections were stained with Safarin-O. Semi-quantitative assessment was made using the Mankin Scale.

The results of the visual inspection, histology, mechanical testing and streaming potential were compared to probe impedance measurement on the graft sites.

3.2.2 Results

Visual

At necropsy, it was observed that the defects were 90-100% filled with repair tissue that was grossly distinct from the adjacent uninvolved tissue. Moreover, we observed in all the dogs in this study that the proximal tissue surface was slightly uneven while the distal repair tissue was smoother. An example of the difference in surface texture between the proximal and distal grafts may be seen in Figure 3.6.

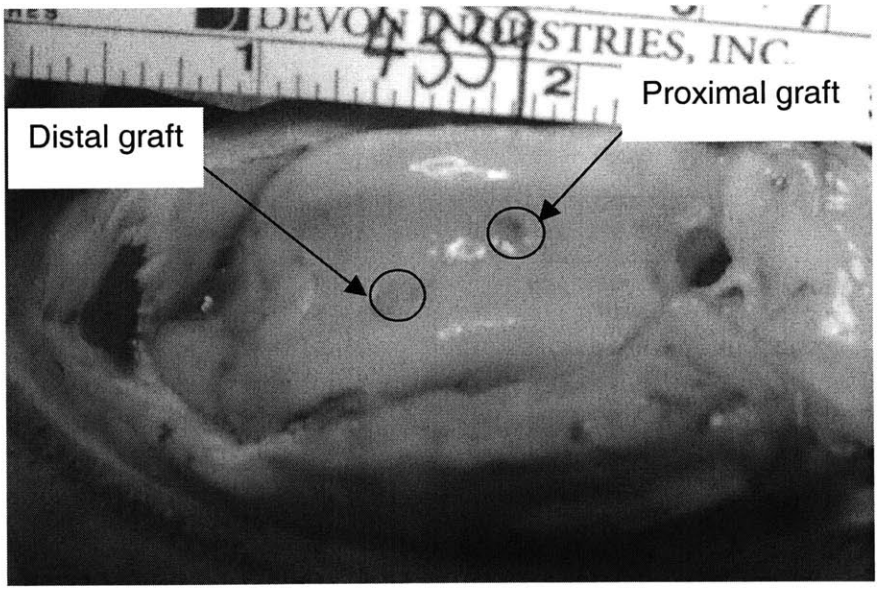

Figure 3.6 Typical surface textures of distal and proximal repair sites. In the dogs in this study, the distal graft tissue was smoother than that in the proximal graft.

Mechanical and electromechanical Measurements

Obtaining mechanical stiffness measurements proved problematic due to the softness of the tissue grafts and subchondral bone. The data was analyzed under the assumption that the bone may be modeled as infinitely stiff compared to the cartilage. In the repair tissue however, the osteochondral bone was undergoing remodeling and was softened, so it was hard to differentiate the measurement of the bone from the measurement of the cartilage. For both equilibrium and dynamic stiffness, the repair tissue was much less stiff (Figure 3.7, Figure 3.8). The electromechanical response streaming potential was negligible.

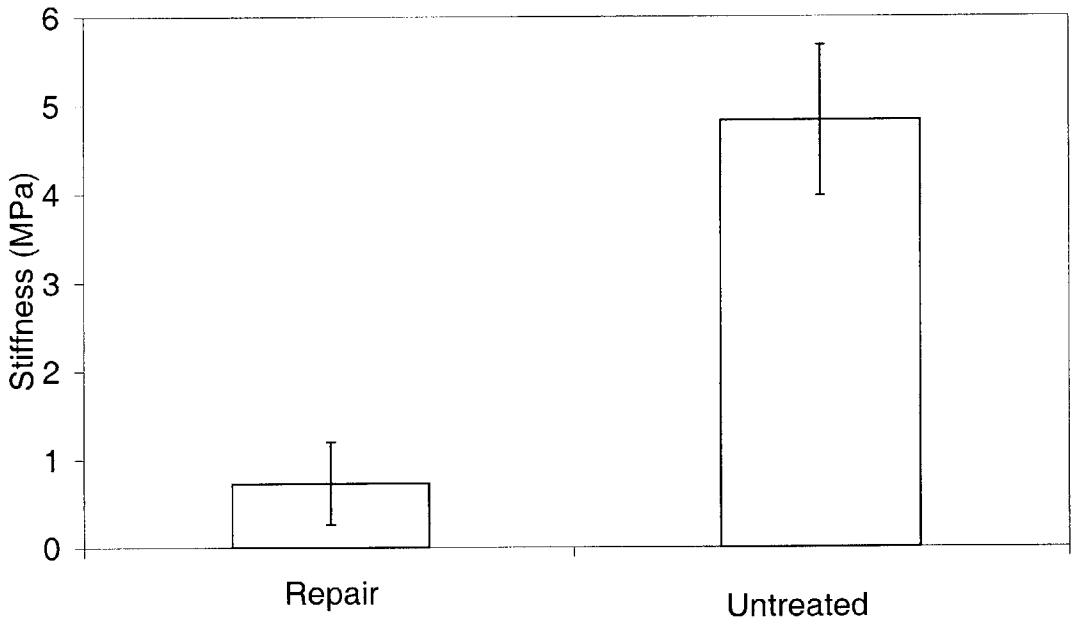

Figure 3.7 Equilibrium stiffness. Repair osteochondral cores were much less stiff under equilibrium loading than untreated samples. Adapted from C. Lee.

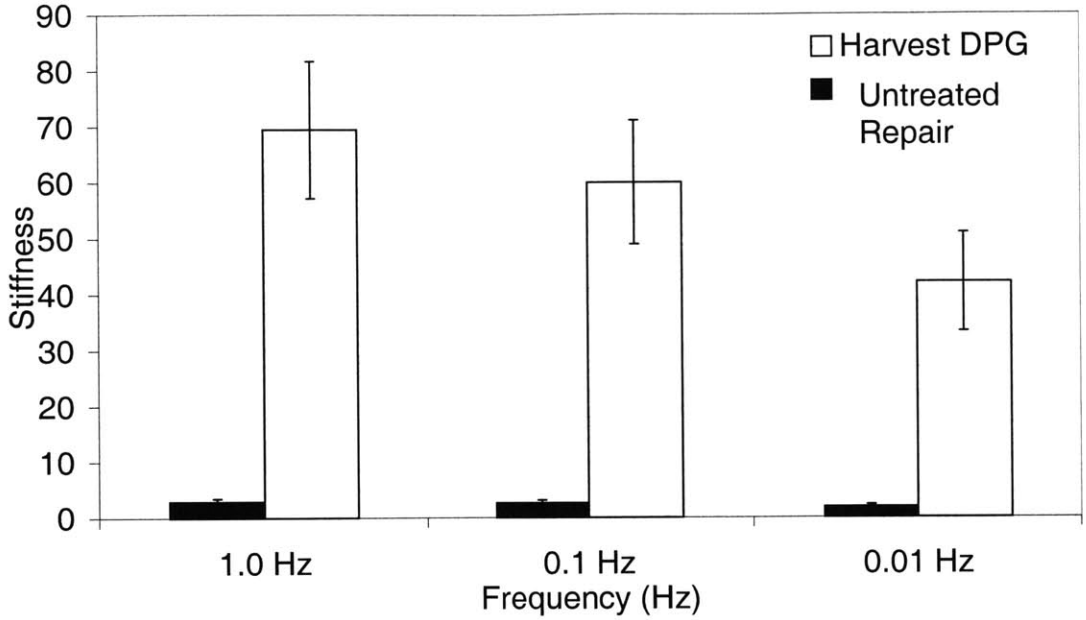

Figure 3.8.Figure 3.9 Dynamic stiffness. Repair osteochondral cores were much less stiff under low-frequency dynamic loading than untreated samples. Adapted from C. Lee.

Histology

The proximal graft from each subject was reserved for histological staining. The repair tissue was found to be predominantly fibrous tissue and fibrocartilage (Figure 3.9).

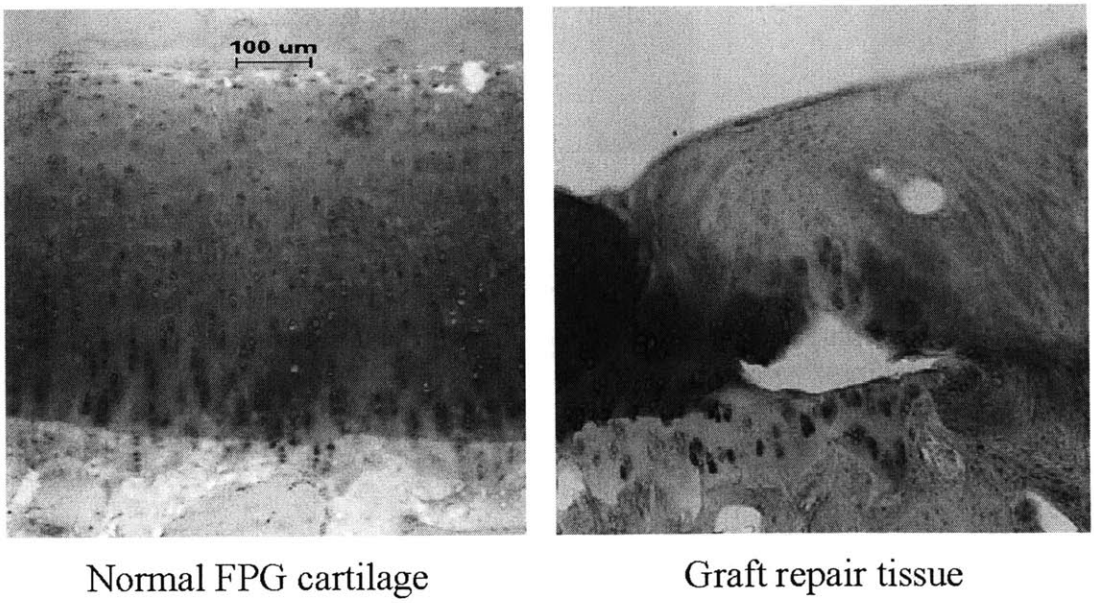

Figure 3.9 Normal canine femoral patellar groove cartilage (left) and typical graft repair tissue composed primarily of fibrous tissue and fibrocartilage (right). Both sections stained with Safarin-O.

Impedance

Figure 3.10 shows the averaged impedances of the proximal and distal graft sites, and the adjacent graft tissue. The graft site impedances were less than that of the adjacent tissue for each frequency. In particular, the impedance of the proximal graft was significantly less than that of the adjacent tissue at all frequencies. This result is qualitatively consistent with the results in Appendix A, in which the osteoarthritically degraded, less functional tissue had a lower impedance. The proximal graft impedance was also less than the distal graft, corresponding with differences in graft tissue surface condition observed at necropsy.

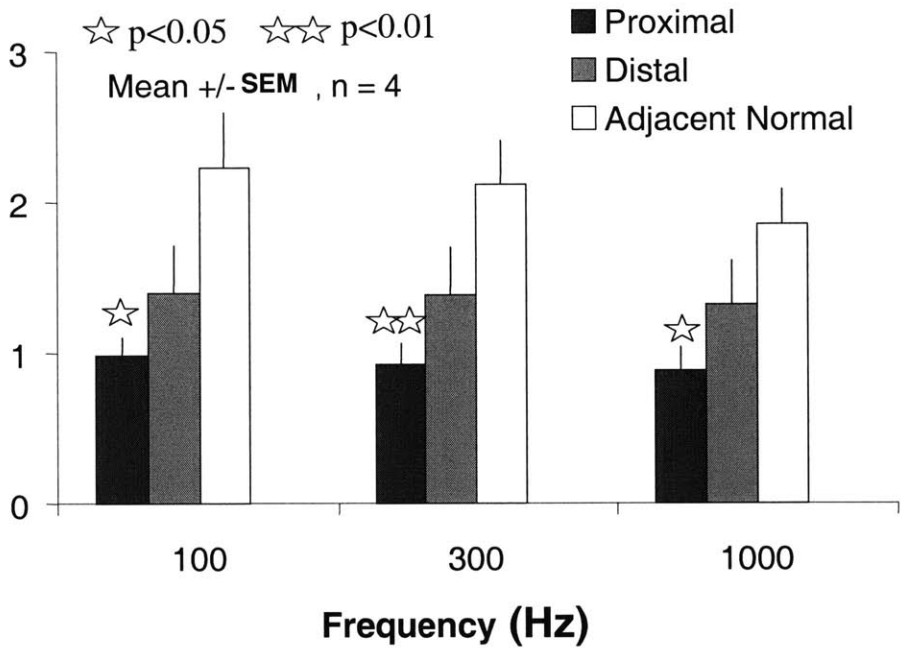

Figure 3.10. Graft tissue had lower impedance than the adjacent normal cartilage. The proximal graft site impedance was significantly lower than that of the adjacent normal, and was also less than that of the distal graft.

3.3 Analysis of Patellar Tissue Articulating Against Harvest and Graft Sites

The next set of experiments was performed on the patellae in order to assess the probe's ability to diagnose the tissue degeneration that may be an indirect result of the surgical procedure. We analyzed the biochemical and electrokinetic properties of the patellae that articulated against the graft sites (right knee) and those that articulated against the harvest site (left knee). A schematic of the test groups may be seen in Figure 3.11. The control group consisted of patellae from dogs that had not undergone any surgical treatment.

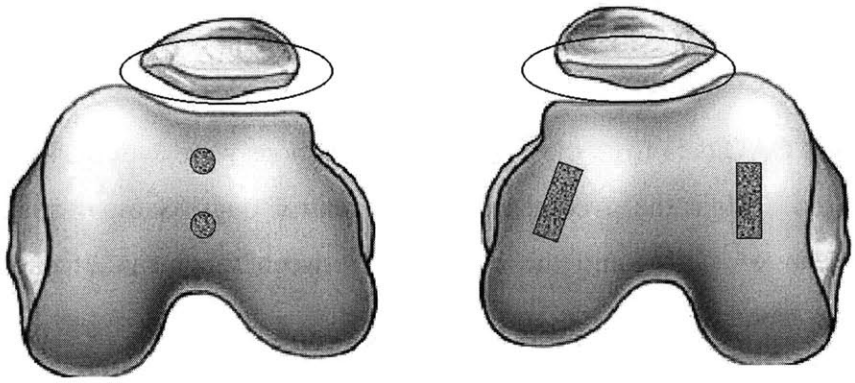

Figure 3.11 Impedance was measured from the patellae (circled) articulating against the graft site knee (dog's right) and against the harvest site knee (dog's left).

3.3.1 Methods

Impedance Measurements

At necropsy, the right and left patellae were excised and wrapped in PBS-soaked gauze. During testing, the patellae were placed in a concave fixture molded from plaster of paris. Impedance measurements were taken by placing the electrokinetic probe on the surface of the patellae with a 50 kPa-offset stress. The electrodes were again configured so that the current penetration depth was 0.7-mm and the current density was 1 mA/cm^2. Tissue

measurements were taken from three different sites on the medial and lateral sides of the patellae. The patellae were moistened with 0.15M phosphate buffer solution during the testing. Immediately before and after each tissue measurement, measurements were taken with the probe in the 0.15M PBS.

Biochemistry

After impedance testing, the patellar tissue was covered with PBS-soaked gauze and allowed to free swell for 30 minutes. A scalpel was then used to remove the articular cartilage from the underlying bone. The cartilage was divided by patellae and by medial and lateral sides. The tissue was weighed wet, lyophilized overnight, and weighed dry. The samples were digested with 2 ml of 200 μg/ml proteinase-K (Sigma, St. Louis, MO) solution at 50° C and aliquots taken to assay for GAG content by dimethylethylene blue dye binding assay.

The hydration and GAG data from the surgically treated dogs were averaged by right and left and compared against the averages from the control dogs. Sample quantities are expressed as mean +/- SEM, and the difference between the mean of samples was assessed by a two-tailed t-test.

3.3.2 Results

No significant difference was found between medial and lateral biochemical or impedance measurements or between the control's right and left patellae measurements.

No significant difference was found in tissue hydration or GAG between the patellae articulating against graft or harvest sites, and there was no significant difference between the hydration or GAG content of the patellae from the surgically-treated dogs and those from the control (Figure 3.12). The impedance measurements were consistent with these results in that no significant difference was between the samples was found (Figure 3.13).

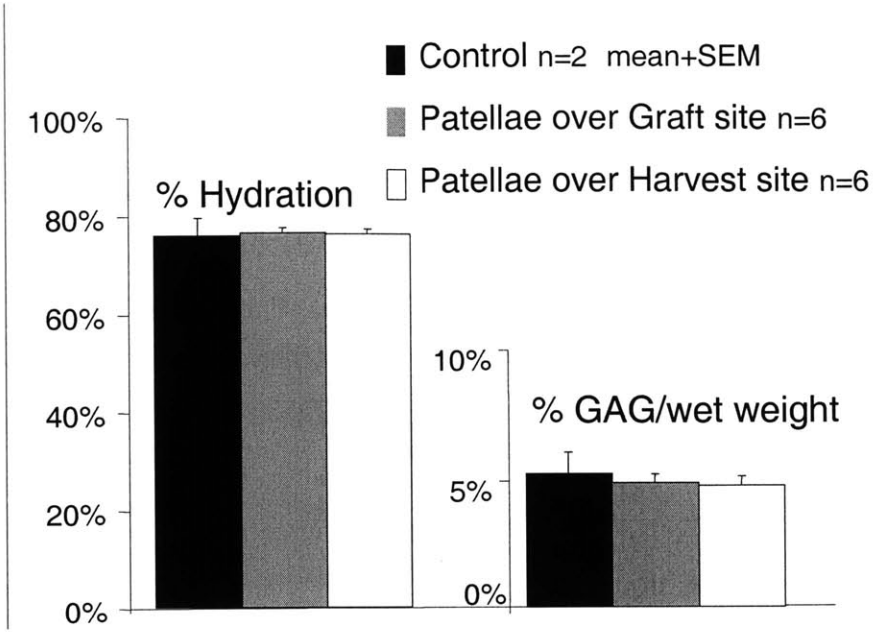

Figure 3.12 The hydration and GAG/wet weight content of the patella over the graft site, over the harvest site, and from the control subjects were not statistically different.

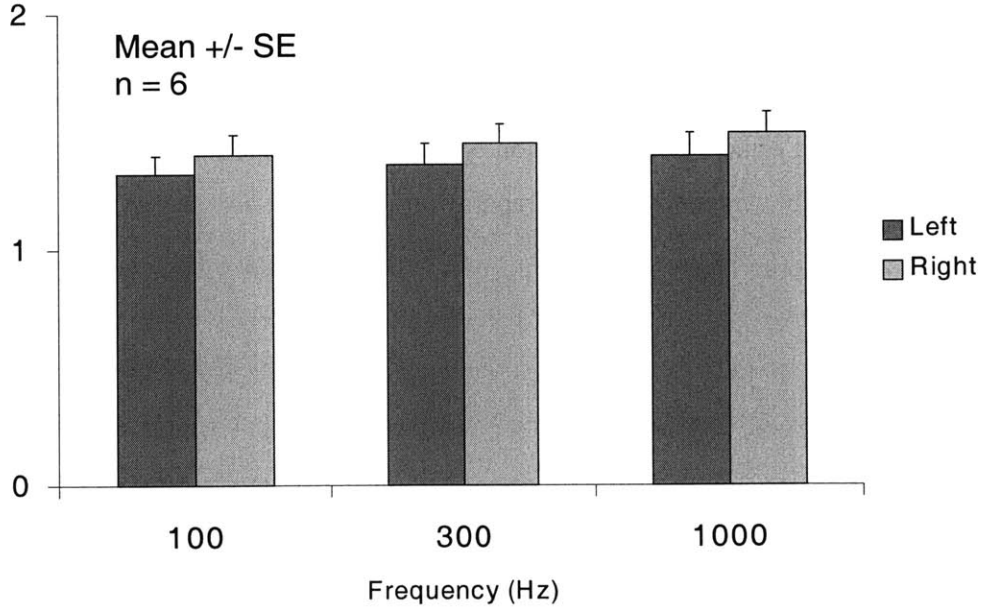

Figure 3.13 The impedances of the patella over the graft site, over the harvest site, and from the control subjects were not statistically different.

3.4 Discussion

In summary, we tested the impedance probe on repair sites on the femoral patellar groove and on patellae articulating against the surgical sites. We found that the impedance in the repair tissue was lower than that in the adjacent tissue. These results corresponded with differences observed in histology and during visual inspection. Preliminary observations further suggest that the graft impedance increases with the percentage of hyaline fill.

For the articulating patellar tissue, no significant difference was observed between the control patellae and those articulating against surgical site. This result corresponds with the relative tissue hydration and GAG measurement and suggests that no significant secondary degradation was occurring in the patellar cartilage at eighteen weeks post-operative.

We therefore see that the handheld probe shows lower impedance in this repair tissue than in healthy tissue. This result is consistent with previous studies on Collins graded human tissue. Moreover, the impedance measurements were consistent with GAG levels, tissue hydration, histology and visual inspection, validating the impedance probe's ability as a diagnostic of cartilage degeneration and repair.

Chapter 4

Effect Of Cryopreservation on Measured Tissue Impedance

4.1 Motivation

An arthroscopic probe for diagnosis of cartilage degeneration and repair is currently under development in the Continuum Electromechanics Laboratory, Center for Biomedical Engineering, MIT. Measurement of cartilage tissue impedance using this probe is an important new modality that may be able to detect early changes in cartilage in diseases such as arthritis. In addition, this diagnostic probe may be useful in following the success or failure of cartilage repair after surgical or drug therapies.

During this stage of technical development, it is sometimes necessary to test specimens that have been previously frozen. The specimens may be from animal models as well as human tissue specimens obtained from collaborating hospitals. It is therefore critically important to determine whether freezing of tissue can significantly affect the measured tissue impedance. The impedance measurements are a function of the content of tissue molecules as well as tissue hydration. The freezing process may affect these molecules and swelling properties.

Deep-freezing articular cartilage is used to limit the synthesis and release of collagenolytic enzymes and other proteinases from the embedded chondrocytes. Dimethyl sulfoxide (DMSO) is often used as a preservative during cryogenic freezing, as this procedure has also been shown to cause severe cellular damage, even as it may preserve network properties [30][42]. Studies indicate that pretreating samples in low concentrations of DMSO inhibits cellular damage for up or 30 months [3], and results in little to no change in matrix organization [48], GAG content [3], limit cycle, or cartilage thickness [22]. However, a study by Alberts et al [1] reports that deep freezing DMSO-

impregnated human cartilage samples for six months decreased the aggregate modulus and increased the permeability over that of samples refrigerated short-term at 4° C.

The bioelectric changes to the tissue during freezing and DMSO treatment and thus the impedance measurements after the freezing process remain unknown. This study proposed to quantify the effects of freezing on impedance measurements, determine the physiological factors that influence any such changes, and determine a method to account for any changes necessary during sample analysis.

4.2 Experimental Procedure

The experiment was carried out as depicted in Figure 4.1 and Figure 4.2 below. Bovine knee joints were obtained from an abattoir, and 9.5 osteochondral cores were extracted from the femoral patellar groove of the knee joints. The surface of the tissue was left intact. The cores were randomly assigned to either be tested for impedance and biochemical properties while still fresh, or after undergoing cryopreservation (CP). The CP group was further broken down into DMSO-treated or untreated groups (Figure 4.1).

The cores were placed in PBS after coring. During testing, the cores were mounted in a fixture and an impedance probe was placed on the surface of the core with approximately a 50 kPa-offset stress. An electrical current of density 1 mA/cm^2 was applied to the surface at a frequency of 3000 Hz. Three different wavelength configurations were used to penetrate approximately 0.7, 1.4, and 2.1 mm into the tissue. Ten iterations were made through the three wavelengths, and 256 measurements were made per wavelength during each iteration. Identical measurements were made with the probe in PBS immediately before and after testing the cartilage tissue, in order to determine the impedance of the electrolyte and the electrode-electrolyte interface. The impedances of groups were recorded as follows:

Z_F fresh group impedance
Z_{Z1} total frozen group impedance before freezing (average of Z_{P1} and Z_{D1})
Z_{P1} PBS group before freezing
Z_{D1} DMSO group before treatment with DMSO and freezing

4.2.1 Biochemical Analysis

One-half of the cores were processed for biochemical analysis after impedance testing as Z_F. Three 0.7-mm slices were taken from the top of the cores. To determine water content of the tissue, each slice was weighed wet, lyophilized overnight, and then weighed dry. The samples were digested with 1 ml of 1 μg/ml proteinase-K solution at 60°C and aliquots were taken to assay for GAG content by dimethylethylene blue dye binding assay. The biochemical measurements were recorded as follows:

H_F fresh group % hydration
G_F fresh group %GAG/dry weight content

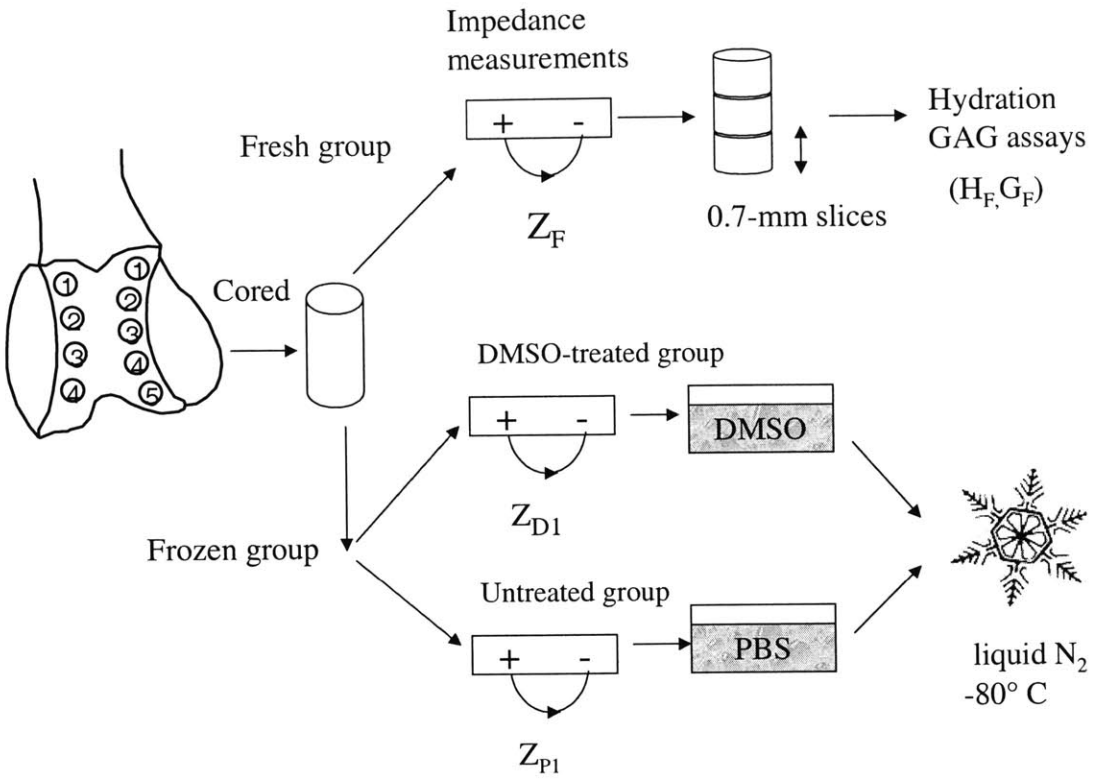

Figure 4.1 Day 1 schematic. The osteochondral plugs were cored and randomly assigned to fresh or frozen groups. The frozen group was further distributed for treatment with or without DMSO. The impedance of the plugs was tested and the fresh group was immediately sliced into 0.7-mm sections and processed for biochemistry. The frozen group was allowed to soak in either 10% DMSO or PBS alone and was then flash frozen in liquid nitrogen and stored for 24 hours at –80° C.

4.2.2 Freezing Procedure

The remaining cores were placed in either 10% DMSO (Fisher Chemical, Fairlawn, New Jersey) or PBS alone for 30 minutes at 4°C immediately after impedance testing, then dipped in liquid nitrogen and stored in -80°C for 24 hours. At the end of the 24-hour freezing period, the cores were allowed to thaw to room temperature in PBS and tested as before using the impedance probe. The impedances of groups were recorded as follows:

Z_{Z2} total frozen group impedance after freezing (average of Z_{P2} and Z_{D2})
Z_{P2} PBS group after freezing
Z_{D2} DMSO group after treatment with DMSO and freezing

The cores were then immediately processed for biochemical analysis. The biochemical measurements were recorded as follows:

H_Z total frozen group % hydration
H_P PBS group % hydration
H_D DMSO group % hydration

G_Z total frozen group %GAG/dry weight content
G_P PBS group %GAG/dry weight content
G_D DMSO group %GAG/dry weight content

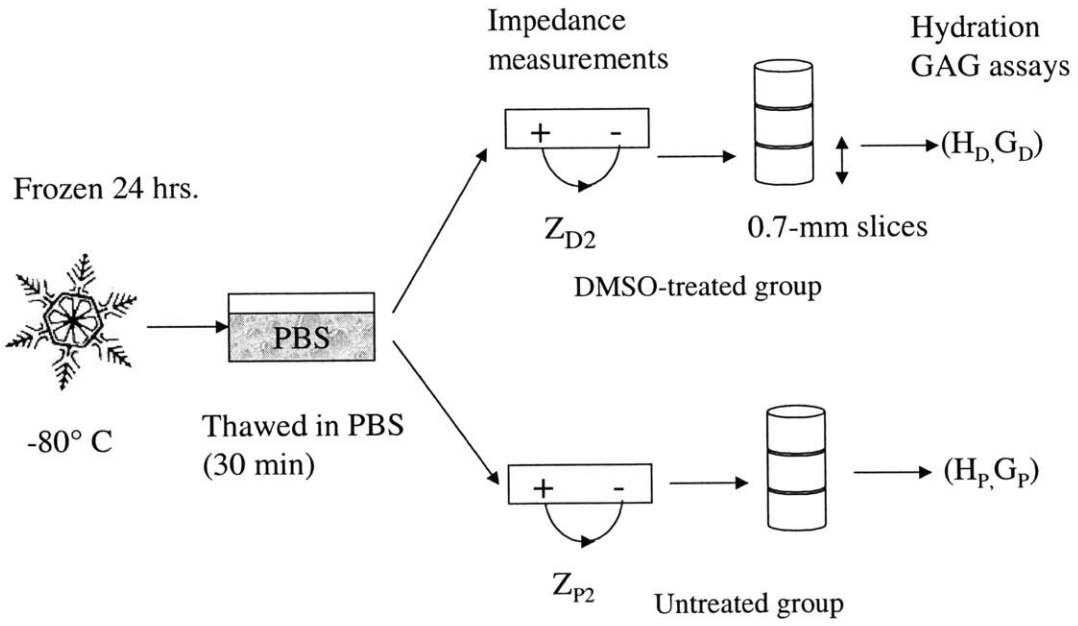

Figure 4.2. Day 2 schematic. The frozen samples were removed from –80° C and allowed to thaw to room temperature for approximately 30 min. in PBS. The impedance of the cores was again measured and both groups were immediately sliced into 0.7-mm slices and processed for biochemistry.

Data Analysis

Linear depth comparison

Due to the destructive nature of the biochemical analysis, hydration comparisons were made among H_Z , H_P, H_D, and H_F, and GAG comparisons were performed likewise. Depth-dependent analysis was performed by comparing the percentages of hydration and GAG per weight of each 0.7-mm slice of tissue (Figure 4.3). The data was presented as mean +/- SE and a two-tailed t-test was used to determine significant differences between the means.

Top: 0-0.7mm Mid: 0.7-1.4 mm Bottom: 1.4-2.1 mm

Figure 4.3 Linear depth comparisons of biological properties.

Averaged depth comparison

The impedance measurements were non-destructive and so Z_{Z1}, Z_{P1}, and Z_{D1} could be compared with Z_{Z2}, Z_{P2}, and Z_{D2}. An average was calculated for the impedance recorded at each penetration depth (short, long, very long wavelengths) and the tissue impedance was divided by the average of the preceding and following measurement in PBS to obtain a normalized impedance for each plug. The measurements were grouped by short wavelength (0-0.7 mm), long wavelength (0-1.4 mm), and very long wavelength (0-2.1 mm).

Biochemical averages were calculated so as to correspond to the short (averaged over the top 0.7 mm slices), long (averaged over the top two 0.7 mm slices), and very long (averaged over the top three 0.7 mm slices) wavelengths. A schematic may be seen in Figure 4.4. Results were presented as mean +/- SE and a two-tailed t-test was applied to determine significance.

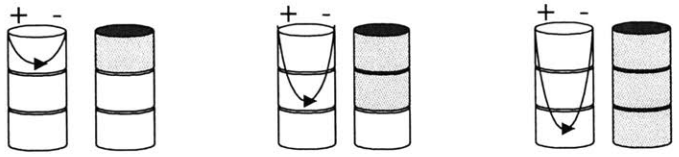

Short: 0-0.7mm Long: 0-1.4 mm Xlong: 0-2.1 mm

Figure 4.4 Depth-averages of the biochemical were calculated for correlation with the three current density penetration depths.

Depth ratio comparisons

To further investigate depth-dependent changes, the short wavelength normalized impedances (NI) were then divided by the long and very long wavelength normalized impedances. Ratios of the depth-averaged biochemical properties were also calculated to correspond to the impedance ratios (Figure 4.5).

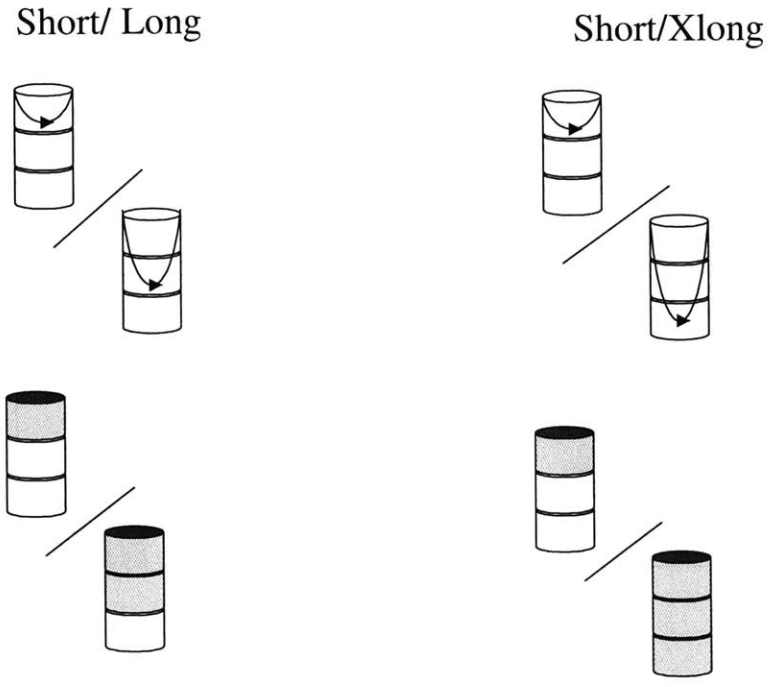

Figure 4.5 Short/long and short/vlong wavelength NI and corresponding depth-averaged biochemical ratios.

4.3 Results

4.3.1 The Effects of Cryopreservation

Linear depth comparison

When the %GAG/dry weight (G_F and G_Z) and the % hydration (H_F and H_Z) were compared on a linear depth basis across the three 0.7-mm slices, no significant differences were found (Figure 4.6, Figure 4.7). There were also no significant depth trends for within fresh or frozen tissue hydration. There may be a trend, though not significant, towards an increase in GAG/dry weight for the fresh tissue (G_F) which was nor present in the frozen tissue (G_Z) (Figure 4.6)

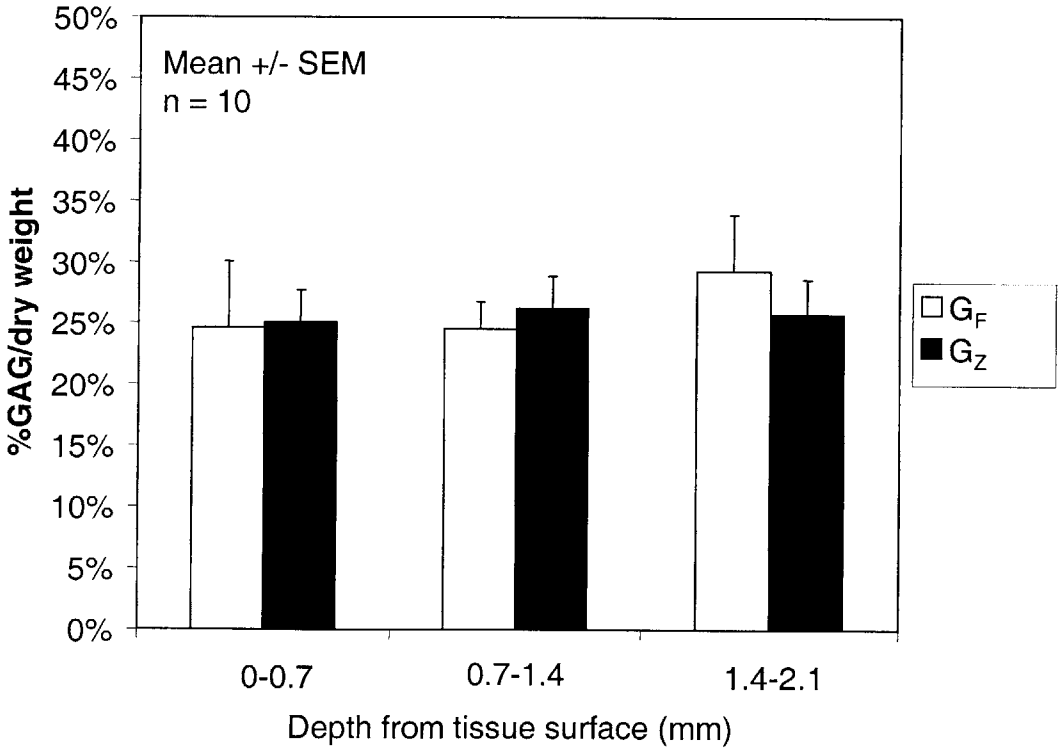

Figure 4.6 Linear depth comparison of %GAG/dry weight. No significant difference on a depth-by-depth basis between fresh (G_Z) and frozen (G_Z). Depth-dependent increase in GAG/dry weight not significant within fresh or frozen tissue.

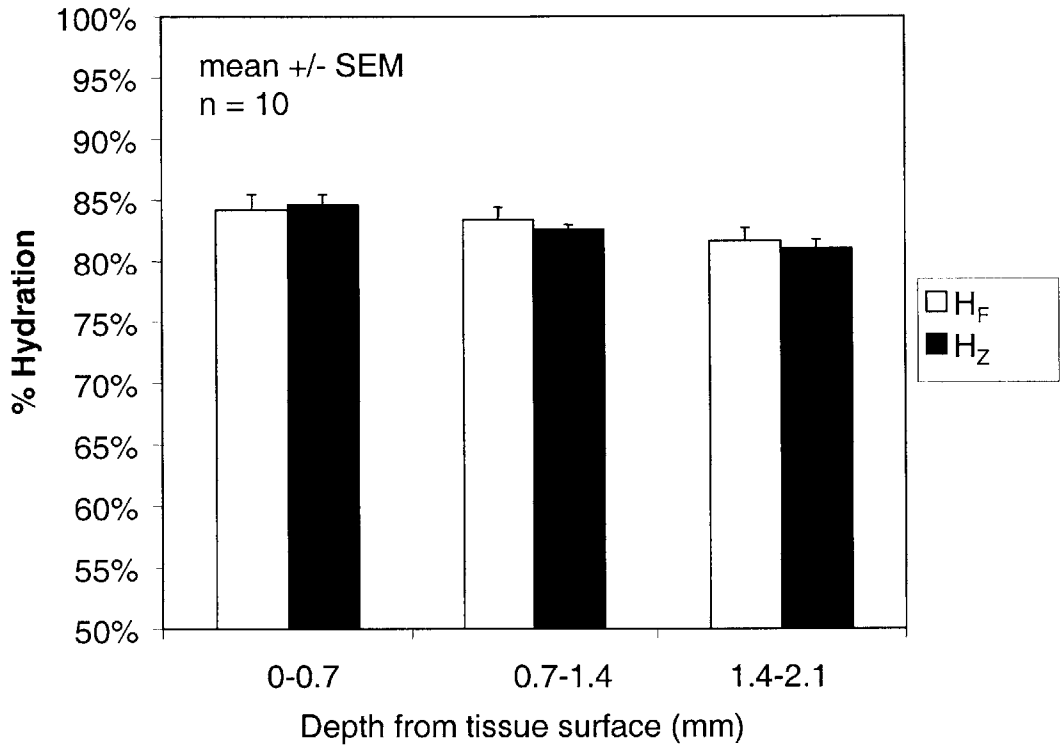

Figure 4.7 Linear depth comparison of % hydration. No significant differences. Decrease in hydration with depth not significant for fresh or frozen tissue.

Averaged depth comparison

When the biochemical properties were averaged together over the three depth intervals, trends emerged. The frozen tissue appeared to have an increasingly less %GAG/dry weight than the frozen tissue as more layers were averaged (Figure 4.8). The frozen tissue also appeared to have increasingly greater % hydration than the fresh tissue, particularly when the top two layers were averaged (Figure 4.9). While these biochemical trends were not statistically significant, the NI was significantly ($p < 0.05$) less in the top 0.7-mm of the frozen tissue than the fresh tissue (Figure 4.10). This depth corresponded to short wavelength configuration. Though not significant, the NI was less in the frozen than fresh tissue for the two other wavelengths. NI differences among wavelength within fresh and frozen measurements were not statistically significant.

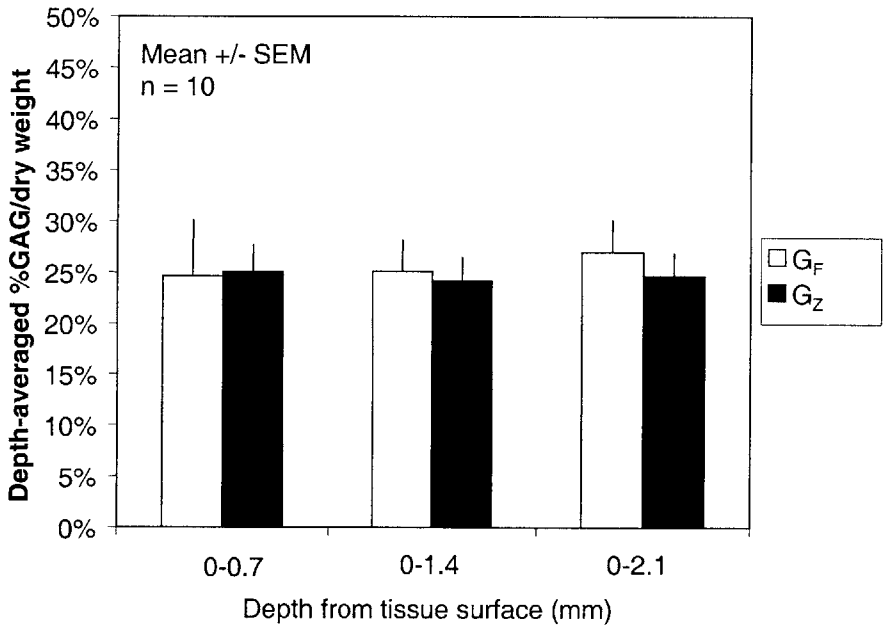

Figure 4.8 Averaged depth comparison of %GAG/dry weight. Trend toward lower %GAG/dry weight in frozen tissue(G_Z), but no significant differences.

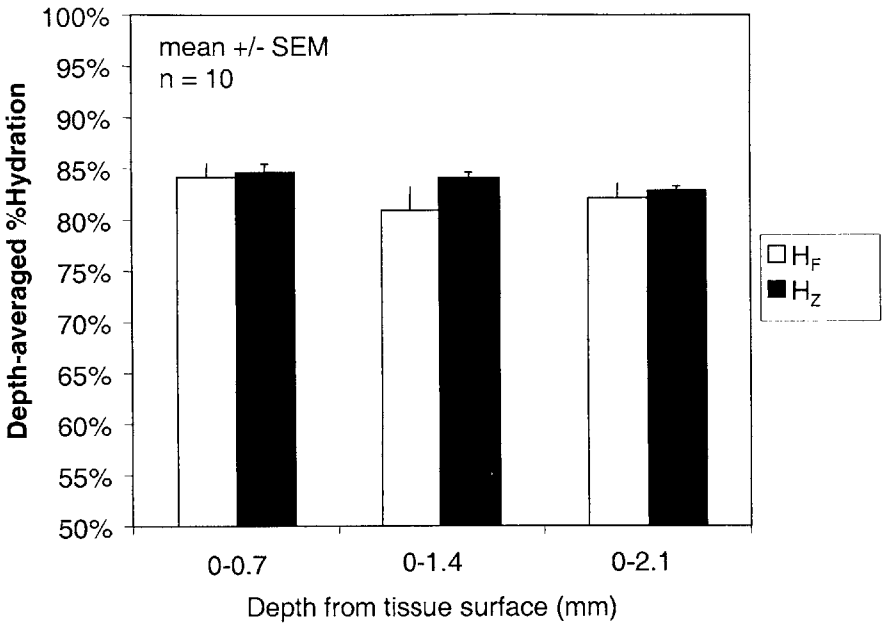

Figure 4.9 Averaged depth comparison of % hydration. Trend toward greater % hydration in frozen tissue (H_Z), but no significant differences.

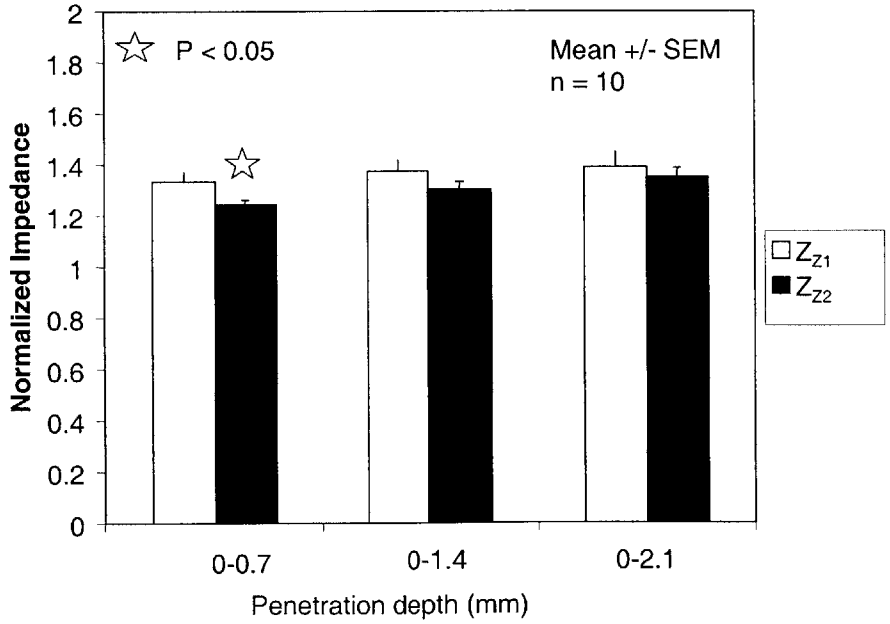

Figure 4.10 Averaged depth comparison of Normalized Impedance (NI). NI less in frozen (Z_{Z2}) than fresh tissue (Z_{Z1}), significant ($p < 0.05$) differences in the top 0.7-mm, corresponding to short wavelength.

Depth ratio comparisons

The % GAG/dry weight depths ratios appeared to be greater for frozen tissue than fresh tissue for both ratios (Figure 4.11). There was a significantly lower ($p < 0.01$) top/mid section % hydration ratio for frozen tissue, while the ratios were approximately the same for the top/bottom section ratio (Figure 4.12). The NI top/mid section ratio was significantly greater ($p < 0.01$) for frozen tissue than the fresh, while the top/bottom section ratios were the same (Figure 4.13).

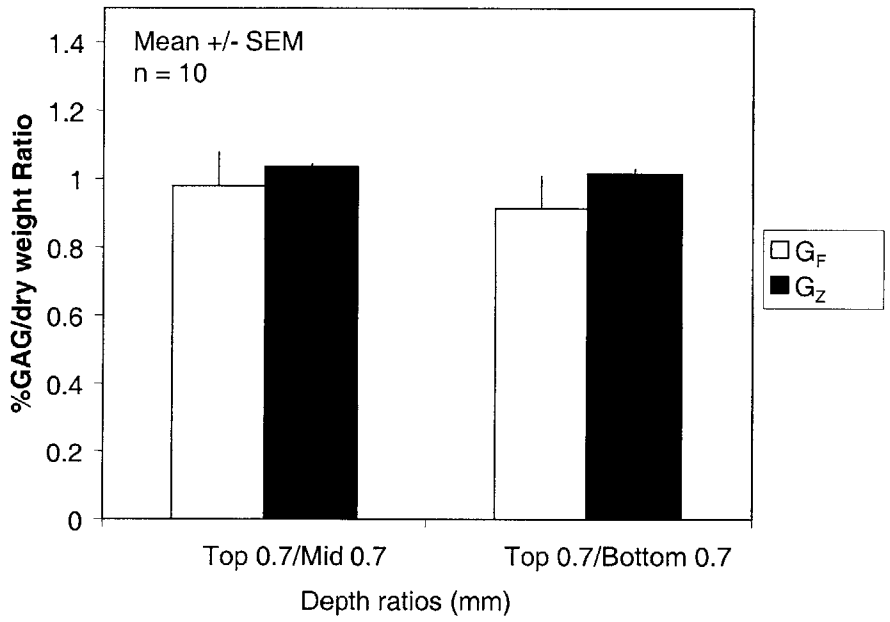

Figure 4.11 Depth ratio comparison of %GAG/dry weight. No significant differences but potential trend toward larger ratios for CG-treated tissue (G_Z).

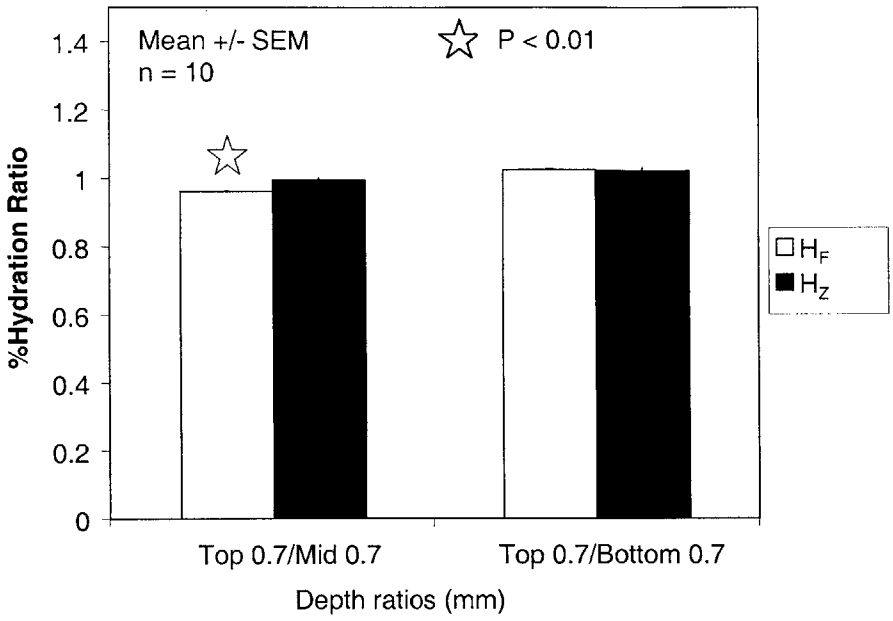

Figure 4.12 Depth ratio comparison of % hydration. Significantly higher ($p < 0.01$) top/mid section ratio for CG-treated tissue (H_Z).

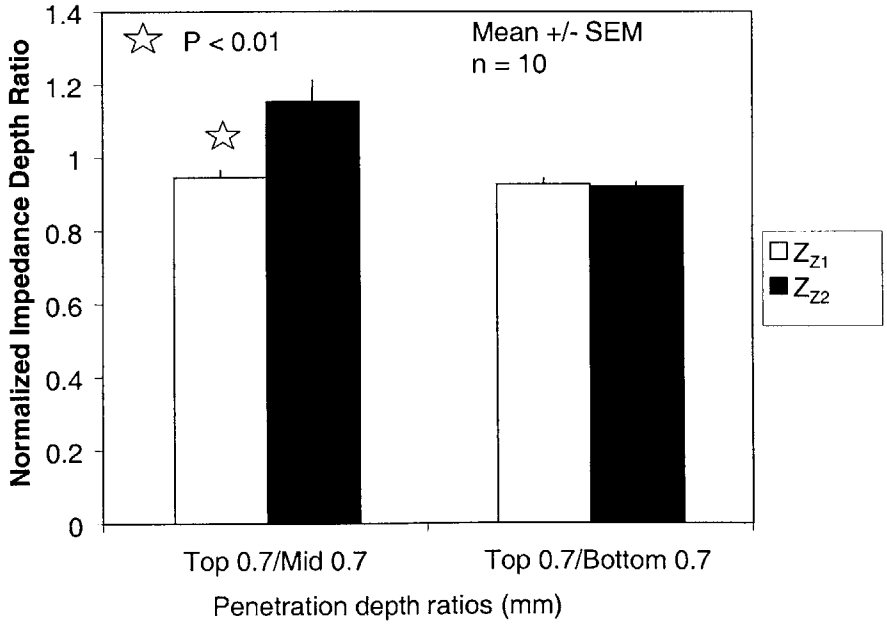

Figure 4.13 Depth ratio depth comparison of normalized impedance. Significantly greater ($p < 0.01$) top/mid section impedance ratio for post-CG tissue (Z_{Z2}).

4.3.2 The Effects of DMSO treatment

The averaged depth properties of DMSO-treated cryopreserved tissue were compared with untreated cryopreserved tissue samples. No trends were found in the GAG levels (Figure 4.14), but there was a significantly lower ($p < 0.05$) water content in the samples in top 0.7-mm of the DMSO-treated samples (Figure 4.15). There was also a trend toward lower NI, that is a smaller increase in NI, in the DMSO-treated samples (Figure 4.16). NI differences among wavelength within fresh and frozen measurements were not statistically significant.

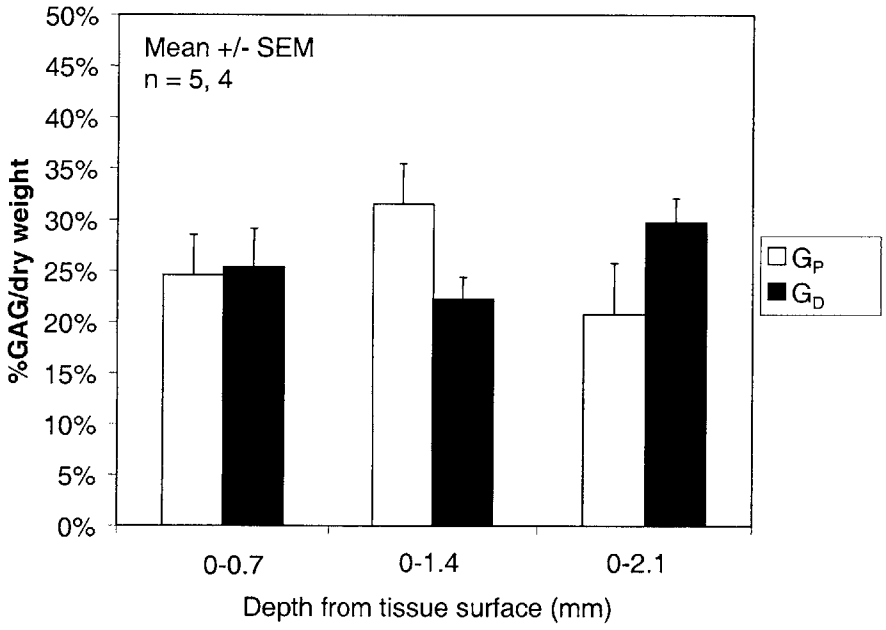

Figure 4.14 Averaged depth comparison for %GAG/dry weight of cryopreserved DMSO-treated (G_D) and untreated (G_P) tissue samples. No significant differences.

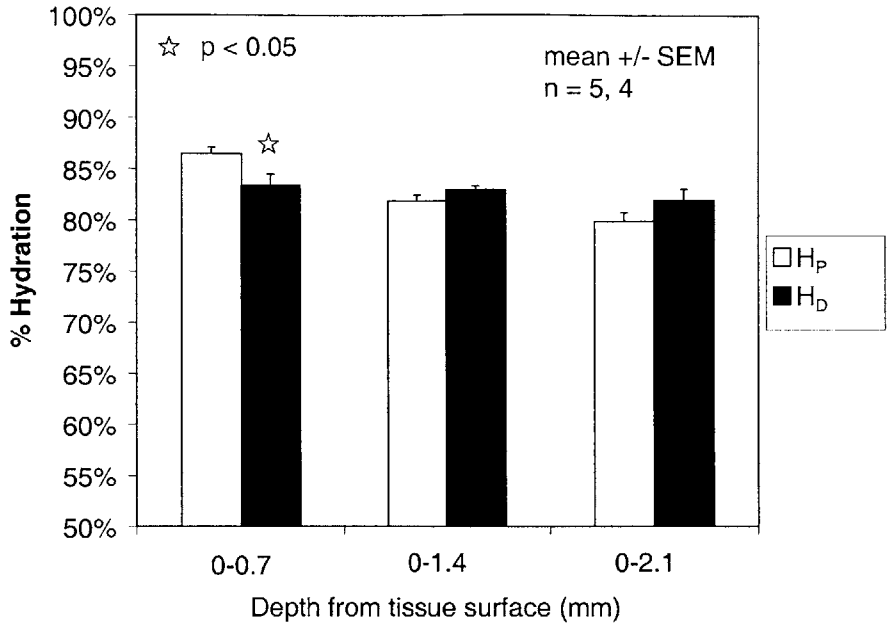

Figure 4.15. Averaged depth comparison for %hydration of cryopreserved DMSO-treated and (H_D) untreated tissue (H_P) samples. Significantly lower ($p < 0.05$) % hydration in DMSO-treated samples in top layer.

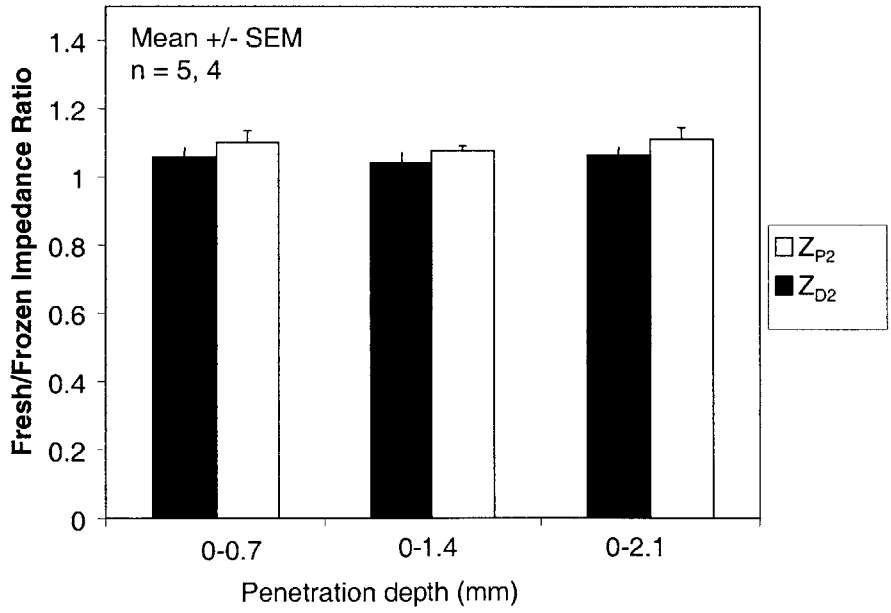

Figure 4.16. Averaged depth comparison for normalized impedance (NI) of cryopreserved DMSO-treated (Z_{D2}) and untreated (Z_{P2}) tissue samples. Trend toward lower NI (less increase) in DMSO-treated samples.

4.4 Discussion

4.4.1 Effects of Cryopreservation

The bioelectric changes in the cryopreserved tissue were similar to those in osteoarthritically degraded tissue. While there were no measurable linear depth-dependent biochemical differences between fresh and frozen tissue (Figure 4.6 and Figure 4.7), there was a trend, though not significant, towards an increase in GAG/dry weight for the fresh tissue (G_F) which was nor present in the frozen tissue (G_Z). Moreover, the depth-averaged comparisons revealed that the frozen tissue appeared to have increasingly less GAG and more hydration than the fresh tissue (Figure 4.8 and Figure 4.9). These biochemical changes corresponded with a decrease in the normalized impedance (NI) in the frozen tissue (Figure 4.10). Because the NI decreased, it may be assumed that the increased depth-averaged hydration dominated the impedance measurement changes.

Depth inhomogeneities appeared when analyzing the depth ratios. Both top/mid and top/bottom GAG ratios appeared to be greater for frozen tissue than fresh (Figure 4.11), which may indicate that the GAG loss was primarily in the superficial layer. The frozen tissue top/mid hydration ratio was lower than the fresh, but the ratios were approximately the same for the top/bottom section ratio (Figure 4.12), which may indicate that the cyropreservation-induced hydration changes in this study were predominantly in the middle section. The frozen NI top/mid section ratio was significantly greater, while the top/bottom section ratios were the same (Figure 4.13), corresponding to the hypothesis that hydration dominated the impedance changes. Further testing is needed to determine if observed trends are significant.

4.4.2 Effects of DMSO treatment

The DMSO-treatment did not appear to affect the GAG levels (Figure 4.14) but appeared to help prevent an increase in surface tissue hydration (Figure 4.15). This reduced

hydration was manifested as a trend toward smaller increase in NI than untreated samples (Figure 4.16). Increased hydration is typically the result of collagen degradation. However, DMSO is not know to directly protect collagen or to inhibit collagenase activity and in fact is used to soften collagen in order to stretch skin during plastic surgery. This effect of DMSO on the tissue hydration merits further investigation.

Chapter 5

Development of an Arthroscopic Electrokinetic Surface Probe with Permanent Electrodes

5.1 Introduction

The surface probe with disposable electrodes (HHv5.0) designed by Treppo [50] and Quan [37] was intended for use in measuring the current-generated stress (CGS) within cartilage tissue. It was then noted that impedance measurements could be taken using the same electrode sensor equipment, and that the quality of the data and the electrode sensor durability were more reliable when measuring impedance. For these reasons, extensive impedance experiments were performed using the HHv5.0 [50]. However, certain parameters designed specifically for measuring current generated stress were unnecessary when measuring impedance and a dedicated impedance probe was designed, manufactured, and tested. The major design criteria addressed were the following:

1. Robust materials. The CGS sensors were designed to be thin (approximately 100μm) in order to allow a piezoelectric sensor to detect the current-generated stress within the tissue. The thinness of the materials rendered the sensors very delicate so that the silver arms could crack or rip upon mounting or with use.

2. Robust assembly. The silver electrodes tended to delaminate from the Mylar shielding due to shear stresses or to the epoxy breaking down with water contact. The delrin sheaths would crack under cyclic loading associated with mounting the new electrodes.

3. Low and variable yield. The photofabrication process used to create the thin electrodes is time consuming and the yield rate can be low. The surface properties of the electrodes would also vary from batch to batch.

4. Sealing. The electrodes would short if water seeped underneath the interchangeable sensor, requiring that the probe be re-sealed for each use. With disposable electrodes, the seal had to be applied by hand and allowed to dry overnight before the probe could be used. Stresses placed on the probe tip during testing would cause the seal to degrade.

The changes in the permanent electrode impedance probe addressed the above issues as follows:

1. Electrodes and insulators constructed from rigid materials. The new electrodes and insulators are sufficiently robust to withstand repeated use at a 50kPa offset stress. This design also frees dimensional constraints on the electrode width, so that they can be machined rather than photofabricated, greatly increasing batch yield.

2. The electrodes contact the surface perpendicular to the longitudinal axis of the silver sheet (instead of parallel). This configuration allowed internal contact between the electrodes and the conducting wires. The insulators may then be positioned in between the electrodes, instead of the electrodes being placed on the surface of the insulator. The electrode-insulator bonding surface is then parallel to the normal stress from the tissue, preventing electrode delamination.

3. Electrodes permanently sealed. Because the electrodes are robust enough to withstand many rounds of testing, they can be permanently sealed inside the body of the probe, preventing solution from leaking into the electronics and causing a short circuit.

5.2 Design and construction

The permanent impedance probe sensor is composed of four silver sheet electrodes sandwiching insulating sheets made of Teflon. The electrodes are hard-wired to

conducting wires leading to the electronics, and the sensor and the connections are encased in a nonconductive, sealing epoxy and housed in a tubular stainless steel body (Figure 5.1).

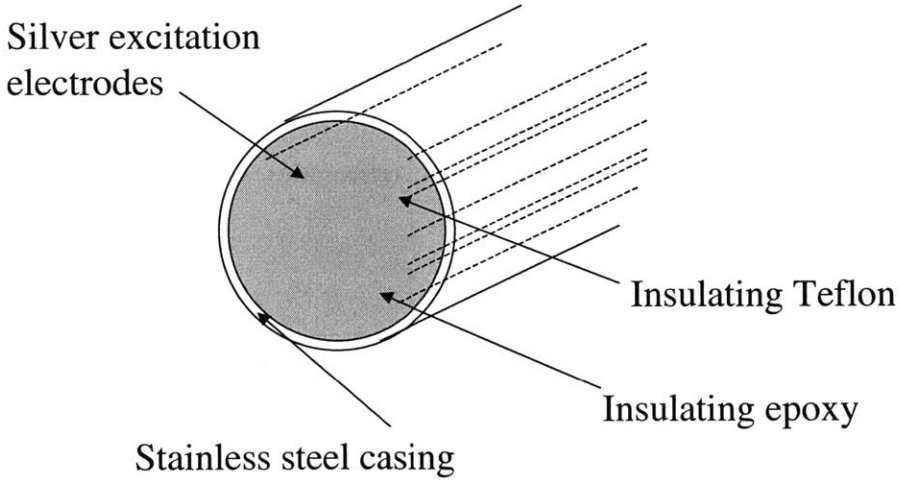

Figure 5.1 Permanent electrode probe. Four silver excitation electrodes are insulated from each other by Teflon sheets and from the stainless steel casing by an insulating epoxy.

Four electrodes (1-mm wide and 4-mm long) were cut from a 0.5-mm silver sheet. Three insulating pieces of the same size were cut from a 0.015" Teflon sheet (Small Parts, Inc, Miami Lakes, FL). The electrodes were sanded and dipped in 15% nitric acid and rinsed in deionized water. They were further washed with a mild detergent and again rinsed in deionized water. A 0.5-mm slot was cut in the tips of each electrode. The electrodes were pressed flat in a vise and a connecting wire was then soldered in place. The spacers were then epoxied (Epoxy-patch, The Dexter Corporation, Seabrook, New Hampshire) between the electrodes in a sandwich-type fashion. The assembly was placed in a vice and allowed to dry overnight. The assembly was then coated with an epoxy shell (Armstrong Products Company, Easton, MA) to isolate the electrodes from one another and placed in an oven at 100° C for 1 hour to cure the epoxy shells. The electrodes were filed to form an even surface and then sanded smooth. The assembly was placed in a stainless steel tubular body.

Electronics for the dedicated impedance probe were the same as for the disposable electrode sensor probe. The computer controlled the current input to the probe through a DAC box to a current source and then to the wire connections.

5.3 Testing of enzymatically degraded tissue

5.3.1 Methods

Experimental Methods

Distal femurs from newborn calves were obtained within hours of slaughter. The femoral patellar groove was isolated, and 9.5-mm diameter cartilage/bone cores were removed from the medial and lateral facets using a coring bit. The cores were sliced to a 6-mm thickness, with at least 3-mm of cartilage. Cores were randomly assigned to be treated enzymatically or as a control in PBS. The enzymatically-treated group was mounted in a confining chamber, such that the enzyme could only penetrate into the cartilage from the flat articular surface. The chamber was sealed in parafilm (American National Can, Chicago, IL) and placed in an incubator at 37° C. The plugs were first incubated at 37° C in 4.64 mg/mL bacterial protease from *streptomyces griseus* (Sigma, St. Louis, MO) in PBS for two hours and then in 0.656 mg/mL collagenase type II (Worthington Biochemical Company, Lakewood, NJ) in PBS for four hours. The cores were then allowed to free swell in PBS for 30 minutes.

Each core was then placed in a cylindrical testing chamber and the tissue impedance was measured with the permanent electrode probe. A sinusoidal current density of $1 mA/cm^2$ was applied to the tissue at 3000 Hz over three wavelengths. The tissue measurements were interspersed with measurements in PBS alone in order to measure the interface impedance.

After the impedance measurements, the cartilage/bone cores were removed from the fixture and allowed to free swell in PBS for 30 minutes. Three 1-mm disks were then

sliced from the top of the articulating surface. The disks were cut in half, and after the excess water was padded away, the wet weight was taken of each. The disks were lyophilized overnight and their dry weights were measured. The samples were digested with 1 ml of 1 μg/ml proteinase-K solution at 60° C and aliquots were taken to assay for GAG content by dimethylmethylene blue dye binding assay.

Data Analysis

Tissue hydration was calculated for each sample according to the formula: 100*(wet weight-dry weight)/wet weight. The hydration percentages were then grouped by depth from the surface of the tissue and the average was taken for each group. The GAG content of each sample was used to calculate both as %GAG/wet weight and %GAG/dry wet. The GAG content percentages were also grouped by depth from the surface of the tissue, and the average was taken from each group.

The impedance measurements for each sample were averaged for each of the three wavelengths. The tissue impedance measurements were divided by the average of the adjacent buffer impedance measurement to determine the normalized impedance at each wavelength. The normalized impedance measurements then were averaged by treatment (enzyme or control) for each wavelength. The difference between the mean of the enzyme-treated tissue properties (hydration, GAG and impedance) and the control tissue properties was assessed by a two-tailed T-test. Results were expressed as mean +/- standard error.

The % GAG/wet weight and % hydration results were then examined for correlation with impedance measurements. The impedance values were correlated with the average % GAG/wet weight and % hydration values of all the tissue through which they passed. Therefore, the long wavelength impedance was correlated with the average of the properties in the two top 0.7-mm sections, and the very long wavelength impedance was correlated with the average of the properties in the three top levels 0.7-mm sections (Figure 5.2).

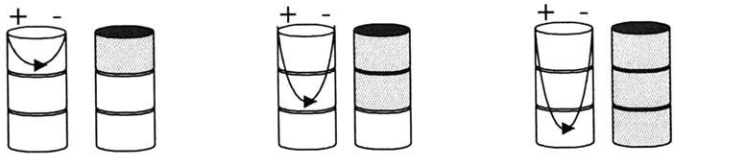

Short: 0-0.7mm Long: 0-1.4 mm Xlong: 0-2.1 mm

Figure 5.2 Depth-averages of the biochemical were calculated for correlation with the three current density penetration depths.

Results

5.3.2 Effects of Enzymatic Degradation

Treatment with pronase and collagenase significantly reduced the amount of GAG in the tissue. Percentage GAG loss as a ratio of dry weight was more significant that as a ratio of wet weight as seen in figures 7-1 and 7-2. The GAG/dry weight in the enzymatically-treated plugs was roughly three times less than that in the controls, and slightly less when calculated as GAG/wet weight.

GAG content was almost constant with respect to depth over the top 2.1 mm of the control plugs, but decreased with proximity to the surface in the enzymatically-treated plugs(Figure 5.3, Figure 5.4). There was a significant increase in percentage GAG/dry weight from top slice to middle slice ($p < 0.01$) and from top slice to bottom slice ($p < 0.05$). The increase in percentage GAG/wet weight was also significant from top slice to middle slice ($p < 0.05$) and from top slice to bottom slice ($p < 0.01$). Change in percentage GAG was not significant from mid to bottom slice was not significant for either GAG/dry weight or GAG/wet weight.

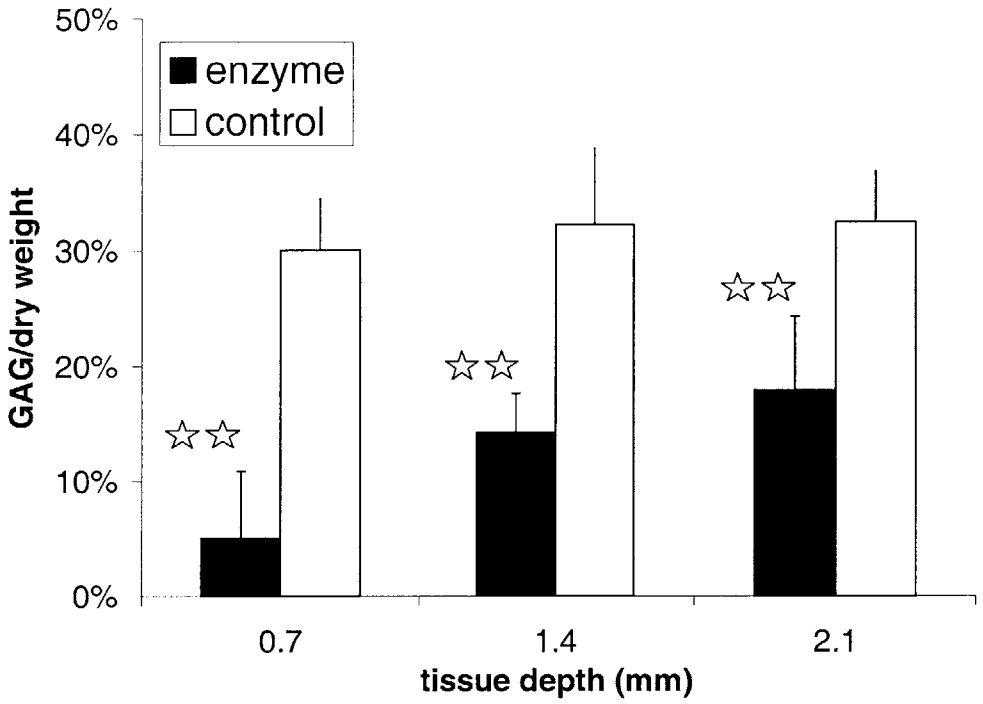

Figure 5.3: Significantly less GAG/dry weight in the enzymatically treated tissue than in the control.

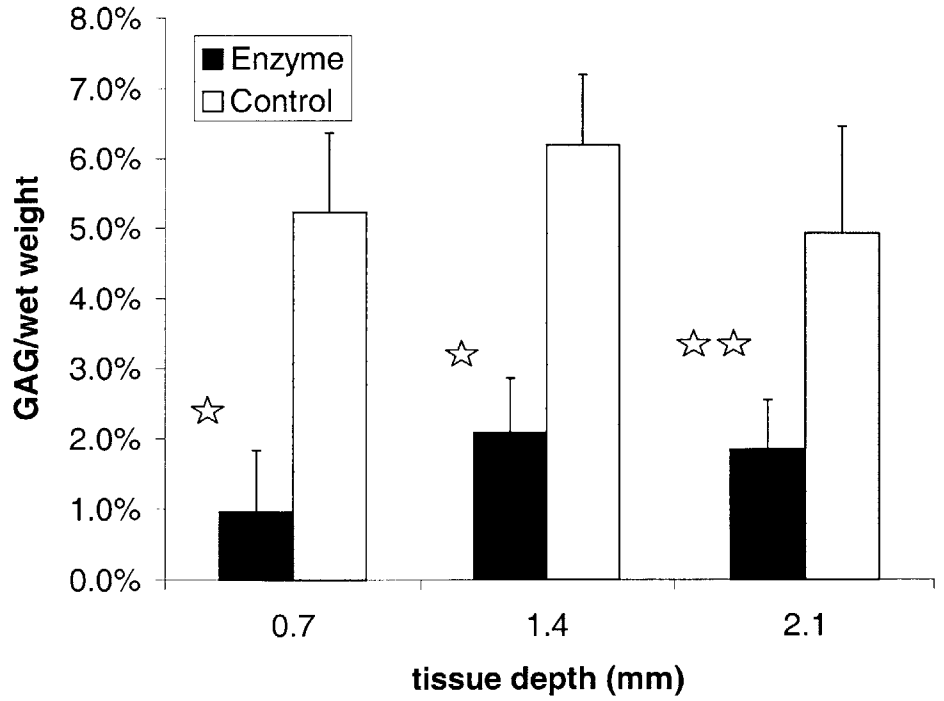

Figure 5.4: Percentage GAG per wet weight of enzymatically-treated tissue is significantly less than control tissue. Significance increases with depth.

This loss of GAG was concomitant with a significant increase in hydration at every depth tested (Figure 5.5). The greatest change in hydration was found in the top 0.7mm ($p<0.01$). The difference in the middle 0.7-mm was less ($p<0.5$), while there was not a significant difference in the bottom 0.7-mm. The depth-dependent change in hydration was not statistically significant for either control or enzymatically-degraded tissue.

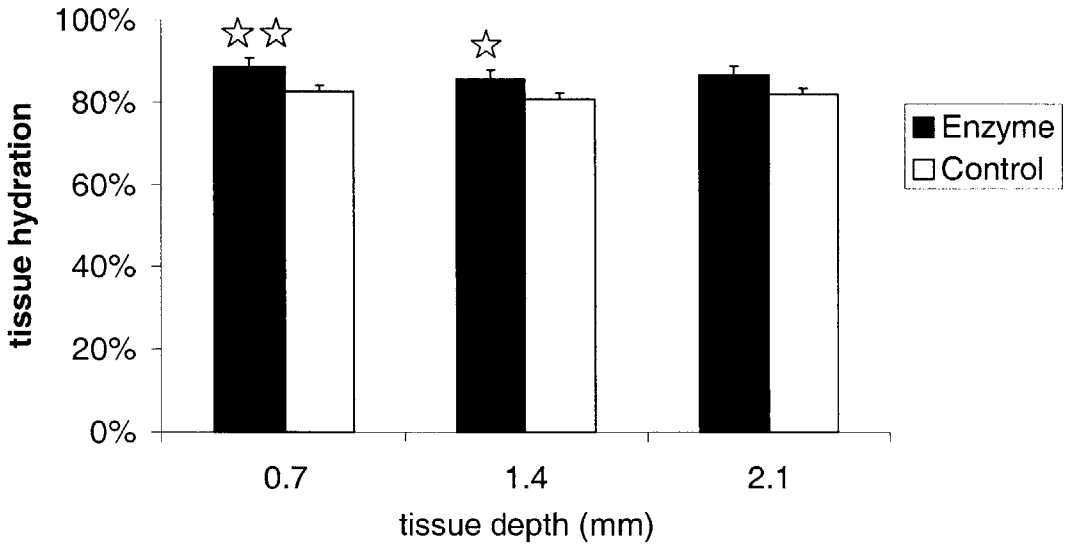

Figure 5.5: Tissue hydration enzymatically-treated tissue compared to control tissue. Enzymatically-treated tissue had a significantly greater hydration near the surface.

5.3.3 Impedance Measurements

The impedance of the enzymatically-degraded cartilage was significantly greater ($p<0.01$) than that of the control at each of the three depths tested as seen in Figure 5.6. The impedance increased slightly with depth for both enzyme and control tissue. The increase in impedance from 0.7-mm to 1.4-mm penetration and from 0.7mm to 2.1mm penetration is statistically significant ($p < 0.05$) in both the enzymatically-degraded and control tissue. The impedances measured in the control tissue when the current penetrated 1.4-mm and 2.1-mm were statistically the same ($p > 0.95$), but not in the enzymatically-treated tissue.

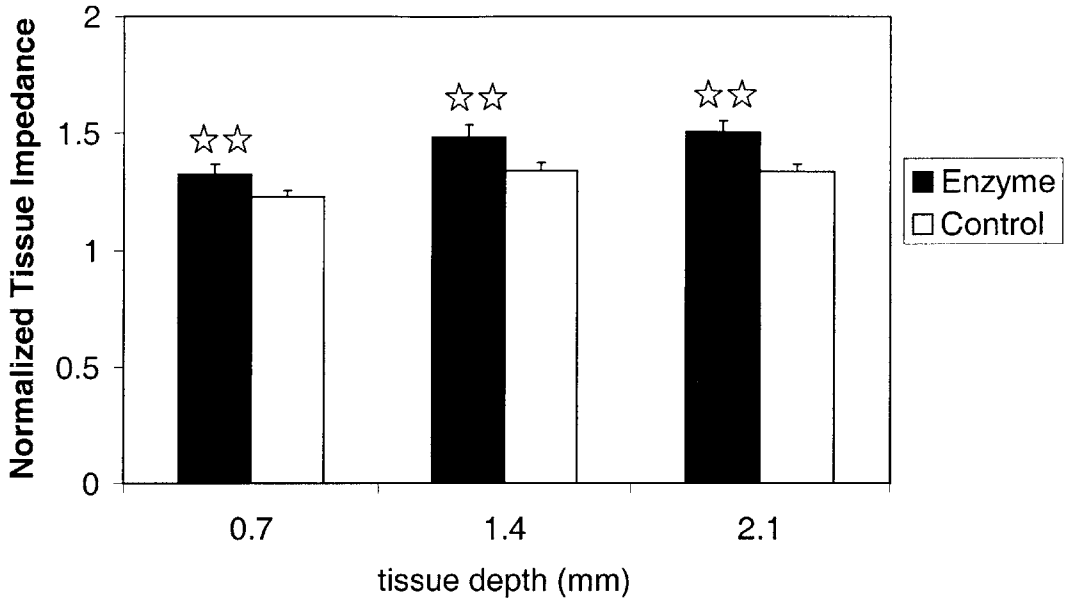

Figure 5.6: Tissue impedance normalized to buffer impedance for enzymatically-treated tissue compared to control tissue.

There was a slight ($r^2 = 0.66$) correlation between hydration and impedance when looking at all wavelengths (Figure 5.7). There was a negative correlation ($r^2 = -0.79$) between %GAG/wet weight and impedance (Figure 5.8).

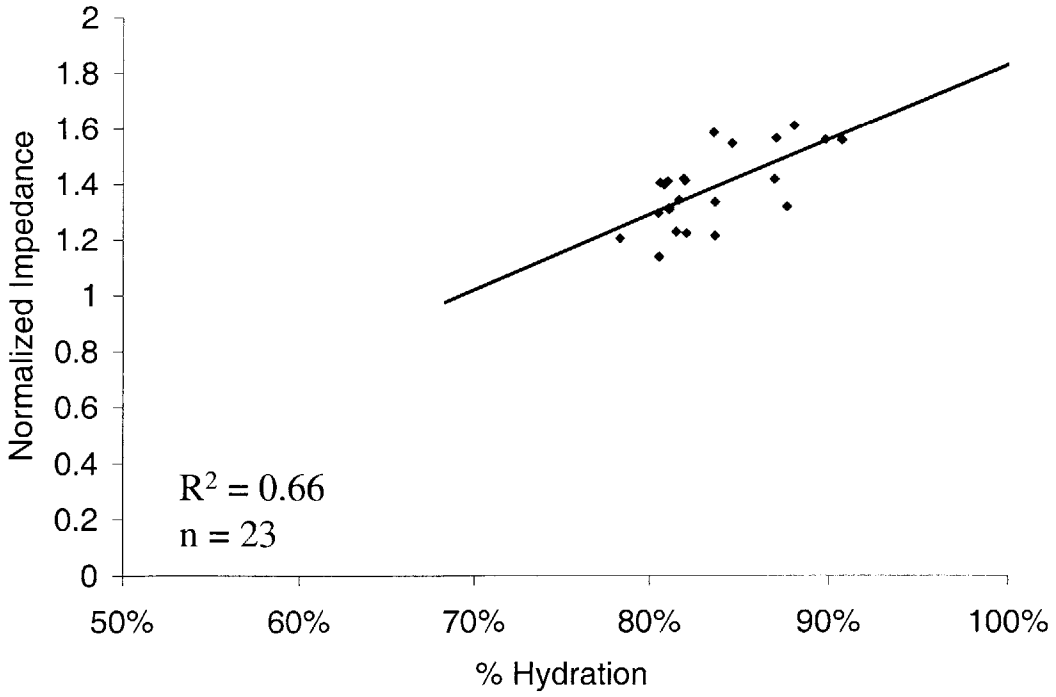

Figure 5.7. A positive correlation between hydration and impedance

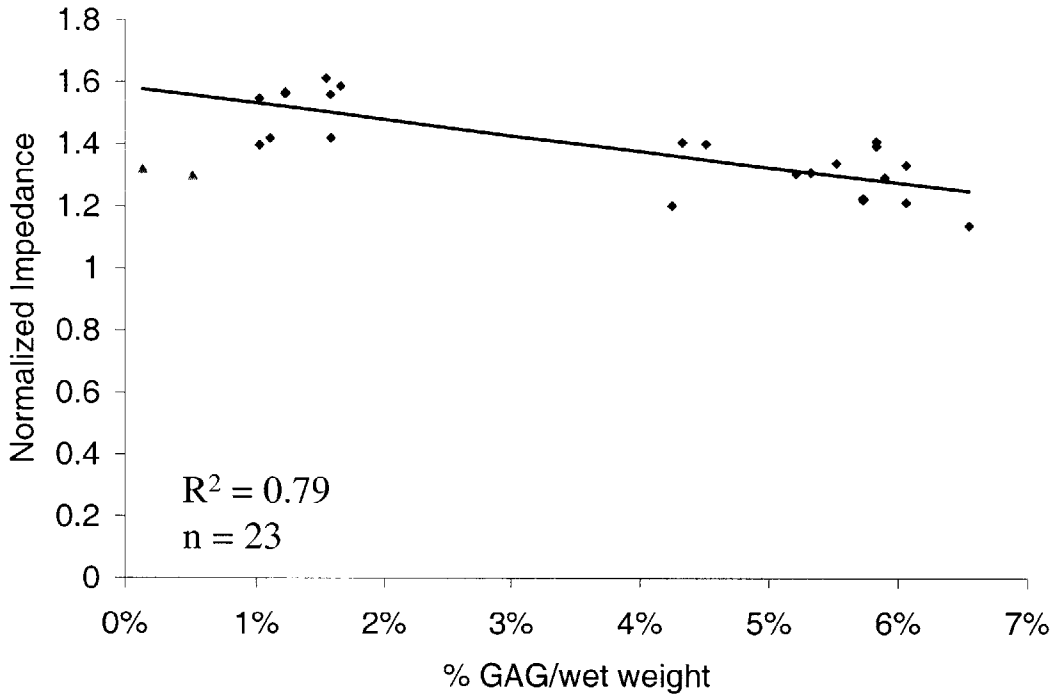

Figure 5.8. A negative correlation (r^2 = 0.79) between impedance and percentage GAG per wet weight. Triangles indicate outliers not included in correlation.

5.4 Discussion

5.4.1 Effects of Enzymatic Degradation

Two significant biochemical changes were induced by the combined pronase/collagenase treatment. The tissue hydration increased and %GAG/wet decreased. These effects were greatest toward the surface of the tissue. The incubation in pronase appears to have begun GAG degradation and the collagenase appears to have fibrillated the tissue so that significant swelling occurred and a significant amount of GAG diffused out into the solution.

This model does not correspond with the effects of osteoarthritis measured in previous studies (see Appendix A), in which the impedance of degraded human tissue was lower than that of healthy tissue. Instead, the significant decrease in GAG and the significant increase in impedance were consistent with previous experiments with trypsin treatment

of newborn bovine articular cartilage. Perhaps if the tissue had been treated for a shorter time in pronase, or with collagenase alone, we would have still seen significant hydration, without as much GAG loss.

5.4.2 Impedance Measurements

The permanent electrode probe did detect the changes in the impedance of the cartilage. The change in GAG/weight appears to have dominated the impedance change in the tissue. A positive correlation was observed between loss of GAG/weight and increase in impedance. This relationship is most likely causal since the loss of the charged GAG molecules would increase the tissue impedance. There was at the same time a slight positive correlation between hydration and impedance. However, this relationship is not believed to be causal, as an increase in hydration would produce a lower impedance. Instead, this result demonstrates the dominance of the effect of GAG loss. While the experiment does not seem to accurately model osteoarthritis, this study shows preliminary evidence that the permanent electrode probe has the ability to discriminate between normal and degraded cartilage.

5.4.3 Permanent Electrode Probe Design

The permanent electrode probe is more user-friendly than the replaceable electrode probe. No user-assembly was required and the user need not test for possible leaks as with the replacement electrodes. The electrodes were sufficiently robust to withstand many tests. This proved to be a great advantage for running many time-dependent tests. When using the replacement electrodes, if the sensor failed through delamination or leaking the tests would have to be postponed overnight till after the sealant had dried and the time-dependent specimens would have to be abandoned. For this reason, the permanent electrode probe was used to test some of the specimens in chapter 5, which had to be tested immediately after procurement and at a 24-hour time point.

Another advantage to this design is that the larger electrodes and perhaps improved surface quality rendered the interface impedance is low enough without chloriding. Eliminating the chloriding step reduces probe-to-probe variations in interface impedance. It is probable that the electrode interface impedance may temporarily change with exposure to tissue, saline, and other factors in the environment. It is therefore recommended that the electrodes be routinely lightly sanded to remove surface deposits.

The permanent electrode probe is also technically simpler to fabricate. The most difficult step was aligning the electrodes while they were been bonded to the insulators. In the future, the electrodes and insulators should be machined using a CNC instrument. The improved dimensional accuracy would allow the pieces to be more easily aligned during fabrication, and to increase the accuracy of the current density being delivered. It would hopefully also eliminate the need to re-flatten the silver pieces after cutting.

One mode of failure did appear during prototype testing: an electrode lost contact with the wire. When this would occur with the disposable electrodes, the sensor could be repositioned or replaced. In this case, a new probe had to be constructed. Another contact issue occurred on some probe prototypes when one electrode and only one would become coated during tissue measurement. The impedance would concomitantly increase. Faulty connections were again suspected. Design specifications may be necessary to ensure that connections are strong and protected and that wire pinch points are eliminated.

It is recommended that all future impedance experiments be conducted using permanent electrodes. The permanent electrode probes are compatible with existent hardware and software and carries the same advantage as the replacement electrode probe in that it is able to detect electrokinetic changes in cartilage tissue and that measurements may be taken at high frequencies for instantaneous readings. The design is flexible to be modified for other applications. For example, the electrodes could be made smaller to be used on smaller joints and in small spaces, and more electrodes could be added for more wavelengths to assess different depths.

Chapter 6

Summary

The assessment of clinical repair procedures requires a comparison of the state and functionality of tissue before, during and after surgery. Moreover, successful osteoarthritic intervention relies on early stage diagnosis. A non-destructive diagnostic tool is needed to sensitively measure the functional physical properties of cartilage. Because the collagen fibrillation and loss of superficial proteoglycans that characterize osteoarthritic degradation result in changes in the conducting properties of the tissue, electrical impedance is a sensitive indicator of changes in the biochemical composition and tissue integrity of articular cartilage.

In this thesis, an analysis of the electrokinetic surface probe using an impedance modality was performed. The electromechanical surface spectroscopy probe was used *in situ* on canine cartilage tissue to assess the probe device as a diagnostic of tissue repair and degeneration. We tested the impedance probe on repair sites on the femoral patellar groove and on patellae articulating against the surgical sites and the impedance measurements were compared with histological, mechanical, and electromechanical measurements. We found that the impedance in the repair tissue was lower than that in the adjacent tissue. These results corresponded with differences observed in histology and during visual inspection. No significant difference was observed between the control patellae and those articulating against surgical site. This result corresponds with the relative tissue hydration and GAG measurement and suggests that no significant secondary degradation was occurring in the patellar cartilage at eighteen weeks post-operative. We therefore see that the handheld probe shows lower impedance in this repair tissue than in healthy tissue. This result is consistent with results for Collins grade 2 versus 0 and 1 human tissue in Appendix A. Moreover, the impedance measurements were consistent with GAG levels, tissue hydration, histology and visual inspection, validating the impedance probe's ability as a diagnostic of cartilage degeneration and repair.

During technical development, we have found it necessary to test specimens that have been previously frozen. The freezing process, including saturation in the chemical preservative DMSO may affect these molecules and swelling properties. The bioelectric changes in the cryopreserved tissue were similar to those in osteoarthritically degraded tissue. The frozen tissue appeared to have increasingly less GAG and more hydration than the fresh tissue. These biochemical changes corresponded with a decrease in the normalized impedance (NI) in the frozen tissue. The impedance probe was again able to detect depth-related changes through spectroscopy, which led to a more sensitive and informative diagnosis. The DMSO-treatment did not appear to affect the GAG levels but appeared to help prevent an increase in surface tissue hydration. This reduced hydration was manifested as a toward a smaller increase in NI than untreated samples.

To increase ease of use and measurement reliability, a permanent electrode probe was designed. The permanent electrode probe is constructed with more robust materials in a more robust assembly. This instrument may be produced with a significantly higher yield and measurements are not affected by electrode delamination or fluid-induced short circuits as with the previous replaceable electrode version.

The permanent electrode probe was then validated using an enzymatic model of cartilage degradation. The combined pronase/collagenase treatment induced GAG degradation and collagen fibrillation so that significant swelling occurred and a significant amount of GAG diffused out into the solution. This model does not correspond with the effects of osteoarthritis measured in previous studies but were consistent with previous experiments with trypsin treatment of newborn bovine articular cartilage. While the experiment does not seem to accurately model osteoarthritis, this study shows preliminary evidence that the permanent electrode probe has the ability to discriminate between normal and degraded cartilage through a positive correlation between loss of GAG/weight and increase in impedance.

Appendix A presented the results of Emerson Quan on the measurement and comparison of the degradation of intact human patellar joint surfaces at different stages of osteoarthritis were reported. Significant differences between normal and degraded tissue could be detected using the hand-held impedance probe. Hydration content increased with Collins grade, while GAG/dry weight and normalized impedance decreased. The increased hydration in the degraded tissue resulted in significantly lower normalized impedance. The lower GAG content and higher hydration in the top 1mm mildly degraded tissue caused a dramatic decrease in the short/extra long wavelength impedance ratio. These results demonstrated that the multiple wavelength feature can enable spatial imaging of tissue degeneration. In addition, the impedance probe's ability to detect differences in early stage osteoarthritis renders it a feasible diagnostic for detection of early-stage osteoarthritic degradation.

Finally, appendices B and C contain information about a new design for a handheld spectroscopic probe using current-generated stress (CGS) to diagnose the electrokinetic state of the tissue, a business plan for the disposable-electrode handheld probe that was developed for the MIT $1K contest.

Appendix A

Comparison of degradation of Intact Human Patellar Joint Surfaces at Different Stages of Osteoarthritis via Impedance Spectroscopy

A.1 Introduction

The assessment of clinical repair procedures requires a comparison of the state and functionality of tissue before, during and after surgery. Moreover, successful intervention relies on early stage diagnosis. A non-destructive diagnostic tool is needed to sensitively measure the functional physical properties of cartilage.

Previous studies have shown that electrical impedance is a sensitive indicator or changes in the biochemical composition and tissue integrity of articular cartilage [5][49]. Collagen fibrillation, as well as loss of superficial proteoglycans, characterizes osteoarthritically degraded tissue. In this study conducted by E. Quan, the minimally invasive hand-held spectroscopy probe was used to measure the electrical impedance of the articulating surface of intact joints. The objective was to measure and compare the degradation of intact human patellar joint surfaces at different stages of osteoarthritis.

A.2 Methods

This study was approved by the MIT committee on the use of humans as experimental subjects. Seventeen human patellae were obtained from the Regional Organ Bank of Illinois and kept frozen at 4C. Donor ages ranged between 13 to 70 years and were visually graded either according to the Collins method at 0/1 (normal) or 2 (mild). Joints were mounted and tested in 0.1M phosphate buffer solution with 0.01M ethylenediaminetetraacetic acid (EDTA), pH 6.5.

Impedance was measured at four sites on each patella. To ensure electrode contact, the probe was held flush to the tissue surface using a constant force spring to apply a small

50-kPa tare stress. A sinusoidal current of density 1mA/cm^2 was applied to the tissue in the higher frequency range (1000, 500, 250 Hz) and at three spatial wavelengths, so that the current penetrated 0.7, 1.4 and 2.1-m into the tissue as seen in figure 1.

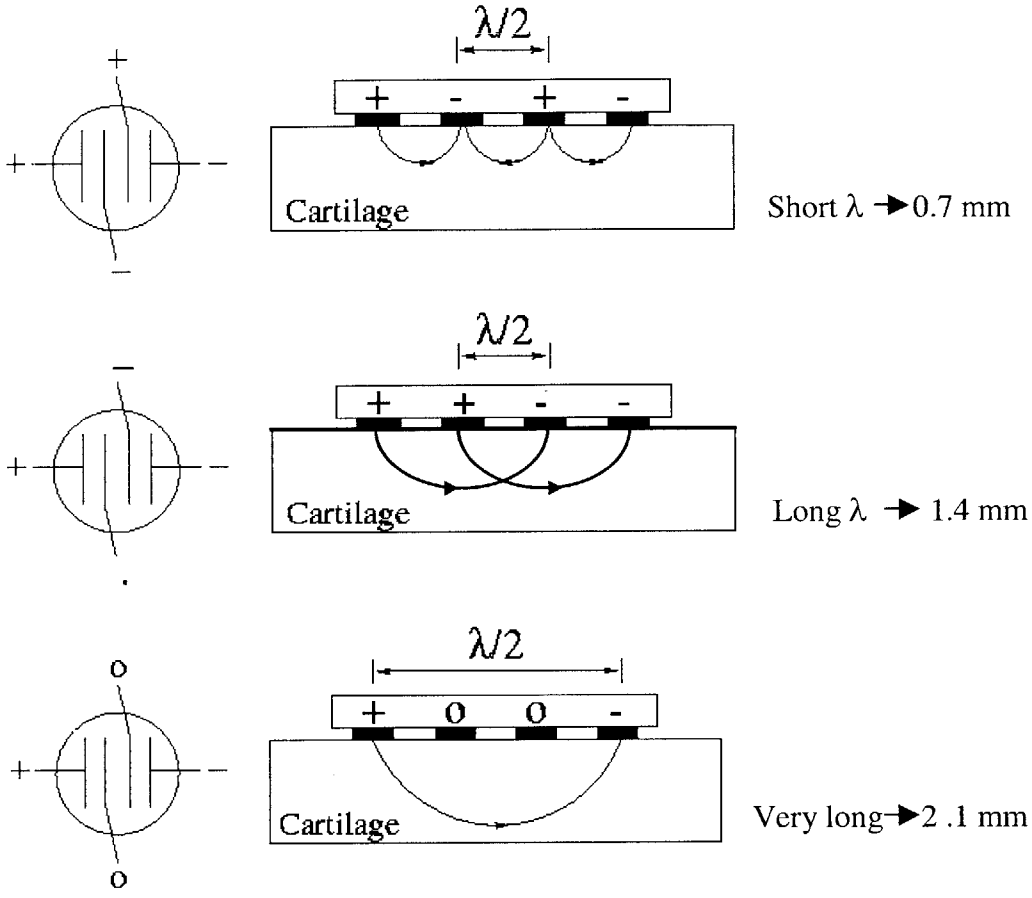

Figure A.1 Short/x-long normalized impedance ratios. Adapted from E. Quan [36].

Tissue impedance was calculated as the measured electrode voltage divided by the driving current, and was normalized to the bathing solution. The tested sites were cored and the top 1-mm layer of the articular surface and the subsequent cartilage layer to the bone surface were removed for GAG and hydration content analysis. Significant differences were determined using an independent t-test with equal variance as determined by an F-test (95% confidence), and a power test was also conducted. The impedance was also analyzed as a short-wavelength to very-long wavelength response ratio (RR).

A.3 Results

There were significant differences ($p < 0.01$) in the GAG/dry weight among Collins graded samples in the top 1-mm of the tissue, but not in the bottom layer to the bone (figure 2). In the top 1-mm, there was significantly more GAG/dry weight in the Collins 0 than in Collins 1 and 2.

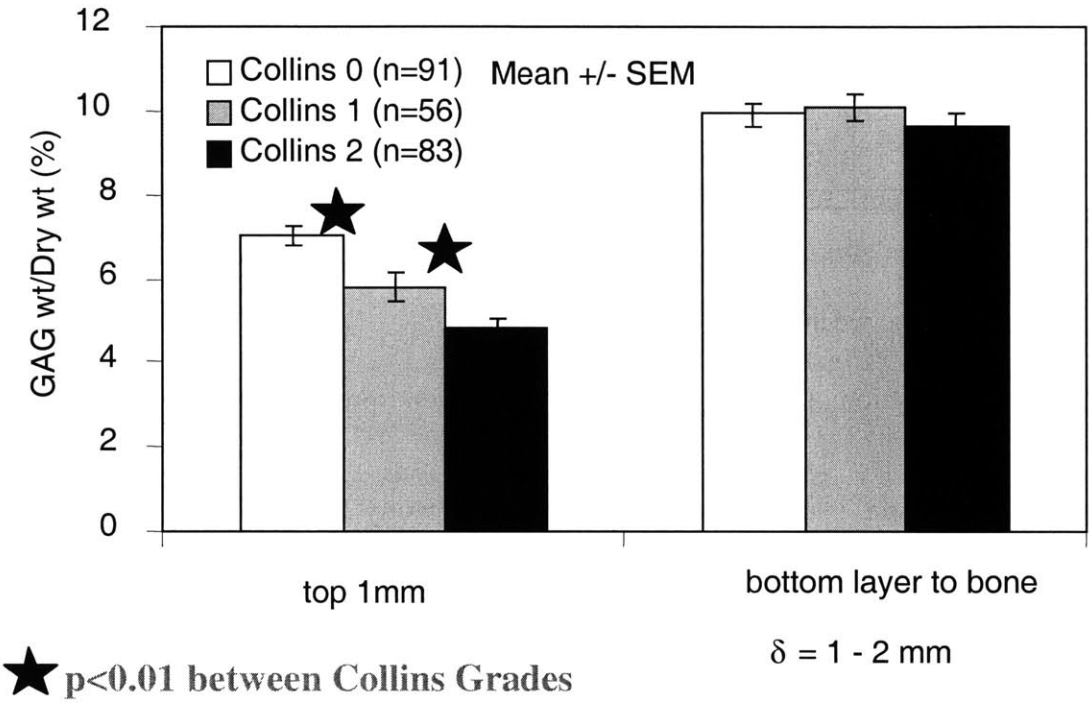

Figure A.2 GAG content of Collins graded tissue. Adapted from E. Quan [36].

Differences between hydration levels were also more significant in the top 1-mm layer than in the bottom layer to the bone (Figure A.3). In the top 1-mm, the hydration in Collins 1 and Collins 2 tissue was significantly greater than that in the Collins 0 ($p < 0.01$). A similar trend was seen in the lower layer, but the difference was not significant.

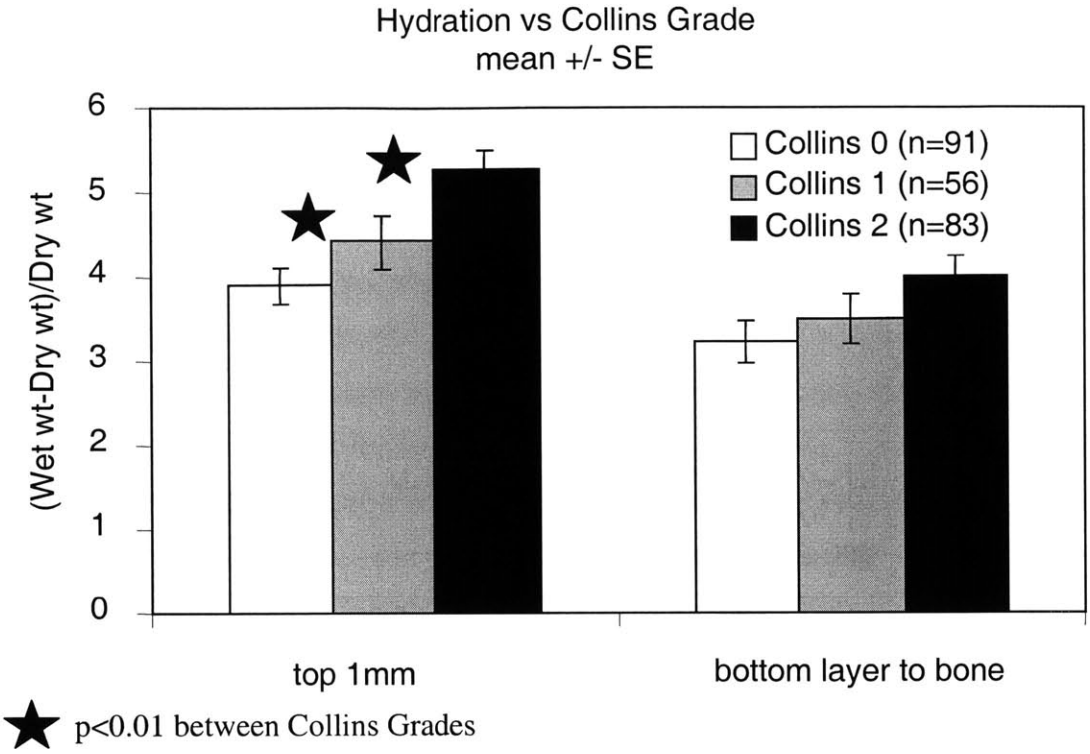

Figure A.3 Hydration of Collins graded tissue. Adapted from E. Quan [36].

The Collins Grade 2 human patellae had a significantly lower normalized impedance compared to normal (Collins Grade 0/1) patellae (Figure A.4). Significant differences were seen using the long wavelength (1.4-mm) configuration at 1000, 500, and 250 Hz ($p < 0.05$). The normalized impedance also appeared to be less for Collins 2 than Collins 0&1 tissue at the short wavelength, but the difference was not significant. The sample size ($n = 10$ for Collins 0&1, $n = 7$ for Collins 2) gave a power of 80% with $\alpha = 0.01$.

The impedance response ratio was plotted over the frequency range (Figure A.5). The Collins 0 and Collins 1, as well as the averaged Collins 0&1 ratios were found to group themselves at a higher ratio than the Collins 2 ratio.

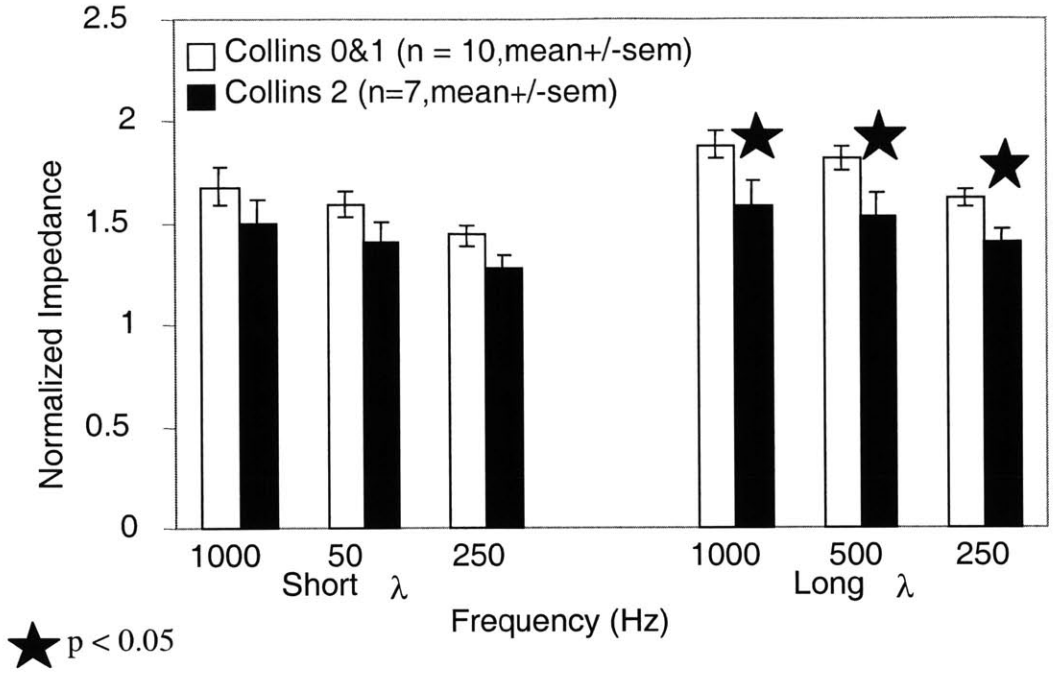

Figure A.4 Normalized impedance of human Collins graded tissue. Adapted from E. Quan [36].

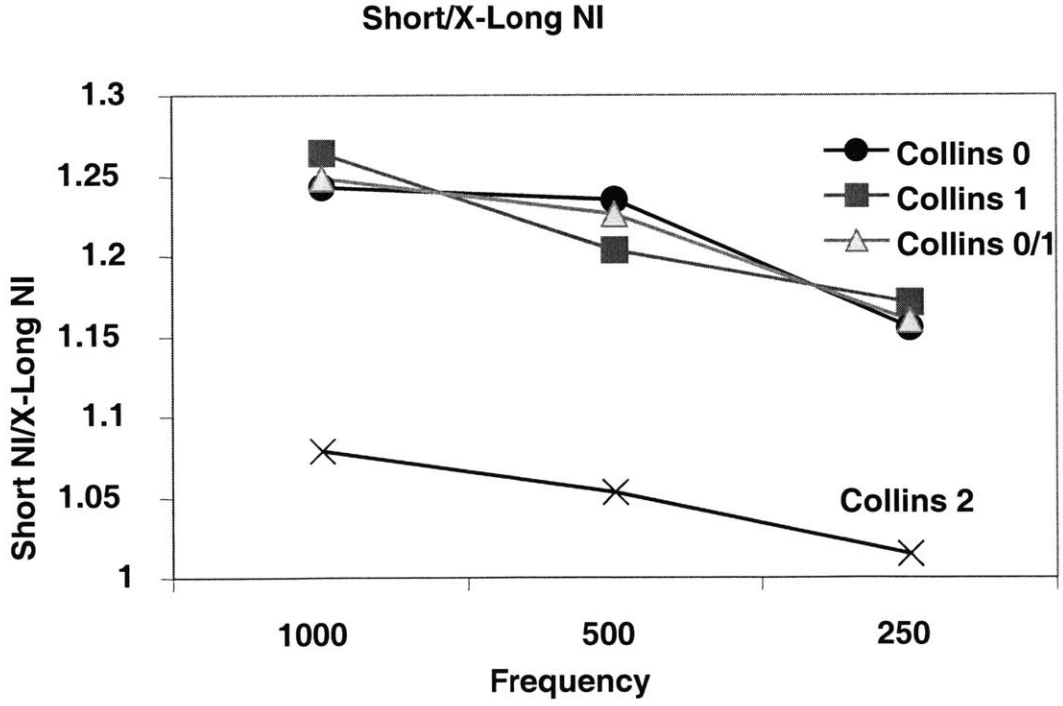

Figure A.5 Short/x-long normalized impedance ratios. Adapted from E. Quan [36].

A.4 Discussion

Significant differences between normal and degraded tissue could be detected using the hand-held impedance probe. The lower GAG content and higher hydration in the top 1mm Collins-2 tissue caused a dramatic decrease in the S/XL wavelength impedance ratio. Hydration content increased with Collins grade, while GAG/dry weight and normalized impedance decreased. The increased hydration in the degraded tissue resulted in significantly lower normalized impedance. This result demonstrates that the multiple wavelength feature can enable spatial imaging of tissue degeneration.

In addition, the impedance probe's ability to detect differences between Collins grade 0/1 and Collins grade 2 renders it a feasible diagnostic for detection of early-stage osteoarthritis degradation.

Appendix B

New Design for a Handheld Probe using Current-Generated Stress Diagnostics

B.1 Current-generated Stress

The probe was originally designed for current generated stress. The probe measured CGS by applying a sinusoidal current to the surface of the tissue using the silver electrodes. The electromechanical coupling in the cartilage produced a streaming potential when the current was applied. The probe measured the stress in the tissue using a piezo. A piezo sensor acted as a dynamic strain gauge that requires no external power source and proportionally converts mechanical stress to voltage.

B.2 Fabrication and Assembly

The CGS sensors were fabricated similarly to the impedance sensors, with the addition of a Kynar piezo. The protocol established by Treppo [50] and Quan [37]was followed. The 4.5 mm diameter sensors are punched from a piezo film and are affixed to the metallized side of the Mylar with conductive silver epoxy (Traduct 2902). Because the piezo is sensitive to voltage inputs as well as stress inputs, the unmetallized side of the Mylar insulates the piezo from the silver electrodes. The metallized side of the Mylar provided shielding by shunting stray currents away from the piezo electrodes to the conducting rim of the inner core, which were in turn grounded to the external electronics. The electrodes on the piezo were photofabricated to exactly correspond with the silver electrodes. The backing plate was attached to the Kynar with two-part epoxy which served to keep the piezo electrodes aligned and flush with the copper contacts on the probe tip.

B.3 New Design for CGS Probe

Certain parameters in the design of the HHv5.0 were assessed with the view of improving signal output and reliability, as well as ease of use. The major parameters addressed were the following:

1. Orientation. Misalignment of the backing plate reduces the conducting area of the piezo and thus impairs the signal amplitude. The piezos are often covered by the used to attach the backing plate. Because the silver electrodes are external, their electrical connections can be checked using an ammeter, but there is no way to assess the piezo connections through tactile or visual feedback for alignment.

2. Ease of assembly. A three-part assembly is required with the replacement of each sensor. Mounting the sensor and the delrin sheath proves difficult because the pieces are small and fragile. Once assembled, they can be difficult to separate.

3. Sealing. The probe must be sealed by hand after each assembly and the sealant must be allowed to dry overnight. If the seal breaks down and water seeps in, the piezo sensor will be shorted to the silver electrodes and will produce a parasitic signal.

4. The probe is placed against the tissue surface with a 50kPa offset stress. The current visual indication of the correct stress is a marking on the side of the probe which can be difficult to read while taking measurements.

The above parameters were addressed as follows (figure A.1):

1. Fewer assembly parts. The sensor will be pre-mounted inside a plastic sheath, also disposable. There will be no outer stainless steel tube. The interchange of these disposable cartridges may then occur in a similar manner to that of the Pipettemen^{TM} .

2. Tactile alignment. The disposable cartridges will contain pins for alignment in grooves in the probe body that will provide tactile feedback for the alignment of the piezo and silver electrodes. The sensor itself will be aligned within the disposable cartridge by means of a grooved assembly plunger.

3. Pre-sealed. The pre-mounted sensor will also be pre-sealed. A nonconducting sealing gel will be deposited in a circumferential reservoir in the tip of the cartridge prior to the insertion of the sensor. The sealant will have the opportunity to dry long before the cartridge is placed on the probe body. The position of the reservoir will protect it from normal and shear stresses.

4. Automatic indication of proper offset. A small contact-dependent circuit near the base of the probe will be activated when the probe is placed on the tissue with the correct offset stress as determined by a spring constant.

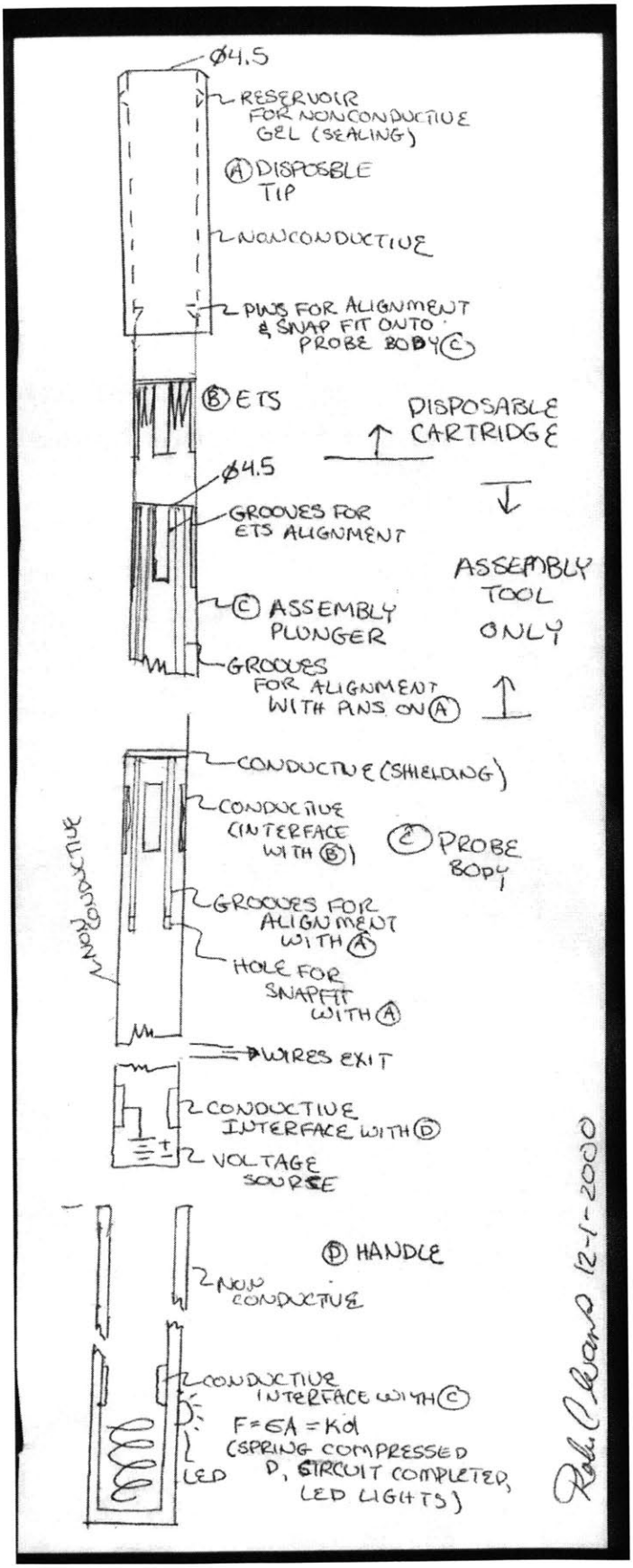

Figure B.1 New design for a handheld current-generated stress diagnostic probe.

Appendix C
Business Plan Summary

"This was one of the most compelling business ideas and plans that I read"
Mike Grandinetti, $1K Entrepreneurship Competition

1 Public Summary

CurrentGenerated (CG) has sole proprietary over a minimally invasive arthroscopic device that has been shown to quantify focal, depth-dependent cartilage degradation. Our current-generated mechanical stress measurements are a significant improvement over the current diagnostic methods, which convey qualitative information and can generally only detect pronounced late-stage osteoarthritis. CG technology allows for early intervention by providing superior detection of early-stage osteoarthritis, and offers critical assessment of therapeutic tissue grafts, drug treatments, and gene therapy.

2 Opportunity Statement/Elevator Speech

Osteoarthritis (OA) is the most common disease that affects the everyday mobility and activities of an individual. CurrentGenerated is developing tools with superior sensitivity for real-time detection of early-stage damage in articular cartilage. CG provides researchers with a tool for developing and assessing therapies, while physicians using our device obtain improved information for earlier intervention.

3 Market Opportunity and Strategy

Osteoarthritis (OA) is the most common disease that affects the everyday mobility and activities of an individual. It is estimated that in the US alone, the number of people suffering from OA will reach 68 million by the year 2010. There is much research going into the development of medical techniques and drugs that could reverse osteoarthritis. As the efficacy of tissue engineering, drug delivery, and gene therapy rises, increasing efforts are being made to diagnose osteoarthritis from its earliest stages in order to determine a treatment before further damage can occur. New cartilage therapies will require tools to assess their efficacy. With viable treatments in sight, the arthroscopy

market has increased to $890.4 million in revenues and is forecast to grow steadily to top $1 billion by the year 2000.

CurrentGenerated takes advantage of the electromechanical transduction properties of cartilage that have been shown to be a sensitive indicator of early matrix degradation. The electric current-generated mechanical stress measurements reveal focal, depth-dependent degradation associated with proteoglycan loss and collagen damage. The CG device is minimally invasive, allowing for fast and simple procedures and quick recovery. The CG provides real-time data in terms of quantitative results that are translated into values easily understood by the physician or researcher.

There are approximately 6,000 hospitals in the United States and 15,000 orthopedic clinics. CurrentGenerated aims to place one base unit in 5% of all hospitals by the year 2005. Due to rising operational costs, there has been a shift towards performing procedures such diagnostic arthroscopy in the clinic office. Private clinics also tend to have more capital for expenditures than hospitals, so CG plans to market aggressive and holds the goal of capturing 10% of all orthopedic clinics as customers. Additionally, we plan on obtaining 2% of the approximately 1,000 companies and institutions that are performing therapeutic orthopedic research. The number of customers in this market will grow as therapeutic techniques improve and more capital is available for research tools.

4 Business Concept

Our revenue model is based on sales of the initial package and subsequent sales of replacement cartridges. The initial package is composed of the handheld device, the hardware, the software, and free on-site training. This package will be offered at 10% profit margin in order to generate interest. The customer will have the option of purchasing for $20,000 or leasing at $550 per month, which would equal the cost of purchase in three years. The primary profits will be generated through sales of sterile replacement electrode tips. A new tip is required for each procedure. We assume the average physician or clinician will need require 100 cartridges per year and the average researcher 50. These items will be sold at 60% profit margin for $500 for a box of 10.

According to market research performed by Frost & Sullivan, the end-users of arthroscopic instruments do not always prefer lower priced products at the expense of quality. Our products are highly differentiated and offer much greater sensitivity, and we would be able to price our products at a premium. Our market analysis predicts 2000 customers over the first five years, generating approximately $10M in revenue from replacement cartridges and $40,000 from the initial package.

CurrentGenerated hopes to obtain Steven Trippel of the Department of Orthopaedics, Massachusetts General Hospital as its primary spokesman. The lab in which CurrentGenerated was developed has worked extensively with Dr. Trippel and we would provide him with company equity in return for using and promoting our product. We also plan to campaign heavily at the Orthopedic Research Society and the International Cartilage Research Society conferences. Our distribution channels will be medical equipment suppliers such as ABC Medical Supplies and the Medical Equipment Corporation.

5 Competitive Advantage

The CurrentGenerated probe offers superior diagnostic sensitivity than other methods on the market. The primary competition lies in radiograph, visual inspection, and mechanical palpation techniques used commonly today. In comparison with these methods, CurrentGenerated electric current-generated mechanical stress measurements provide quantitative information on the biochemical state of the tissue. These methods also only provide information about the tissue surface condition. Histological examination is the primary technique performed in laboratories to further investigate the progression of osteoarthritis. However, this procedure requires a destructive biopsy.

Other quantitative arthroscopic probes have been developed, including an ultrasound probe (Dr. Suh at Tulane University) and a mechanical strain probe (Lyrra et al). However, these techniques solely measure changes in mechanical properties. None

provide the diagnostic sensitive provided by CG's electromechanically coupled measurements.

CurrentGenerated technology has been published in the Journal of Biomechanics and presented at the Orthopedic Research Society and International Cartilage Research Society conferences. There is a patent pending.

6 Team

Robin Evans is a master's student in MIT's Continuum Electromechanics Laboratory where she has been continuing Quan's research and development with the CG probe research and development. Under Evans' tenure, the probe was tested in an in situ surgical setting and used to analyze tissue grafts. Evans is also honing her entrepreneurial skills in Howard Anderson's section of the Sloan School of Management's New Enterprises class.

Emerson Quan is an MIT graduate alum whose master's thesis was on the development of a medical device to better detect osteoarthritis. He has tested prototype devices on human tissue samples to show proof of concept for this technology. His has presented his findings to the Orthopedic Research Society and the International Cartilage Repair Society. Currently he is working at Boeing doing research on decision support software with applications from the aerospace field to medical devices.

References

[1]. Alberts, L Russell; Neff, J R; Bruggeman, N B.; Keenan, S M: Effect of Cryopreservation Technique of the Viscoelastic Properties of Cartilage. Poster Session, 47th Annual Meeting, Orthopedic Research Society, 2001

[2]. Aydelotte MB, Kuettner KE: Heterogenity of articular cartilage and cartilage matrix. In JF Woessner, Jr and DS Howell, editors, *Joint Cartilage Degradation*, chapter 2, pages 37-66. Dekker, New York, 1993.

[3]. Beck O: Preservation of Articular Cartilage. 2. Behavior of glycosaminoglycans (GAG) and the intracellular substance of preserved articular cartilage (histo- and biochemical studies). *Z Exp Chir*, 9(2):96-107, 1976

[4]. Berkenblit SI, Frank EH, Grodzinsky AJ: Spatial localization of cartilage degradation using electromechanical surface spectroscopy with variable wavelength and frequency. *J Orthop Res*, submitted

[5]. Berkenblit SI, Frank EH, Salant EP, Grodzinsky AJ: Nondestructive Detection of Cartilage Degeneration Using Electromechanical Surface Spectroscopy. *J Biomech Eng*, 116:384-392, 1994

[6]. Berkenblit, SI: *Spatial Localization of Cartilage Degradation Using Electromechanical Surface Spectroscopy With Variable Wavelength and Frequency*. PhD Thesis, Massachusetts Institute of Technology, 1996

[7]. Billinghurst RC, Dahlberg L, Ionescu M, Reiner A, Bourne R, Rorabeck C, Mitchell P, Hambor J, Diekmann O, Tschesche H, Chen J, Van Wart H, Poole AR: Enhanced cleavage of type II collagen by collagenases in osteoarthritic articular cartilage. *J Clin Invest*, 99:1934-1545, 1997

[8]. Breinin HA: *Development of a Collagen-Glycosaminoglycan Analog of Extracellular Matrix to Facilitate Articular Cartilage Regeneration*. PhD Thesis, Massachusetts Institute of Technology, Cambridge, MA, 1998

[9]. Brittberg M, Lendahl A, Nilsson A, Ohlsson C, Isaksson O, Peterson L: Treatment of deep cartilage defects in the knee with autologous chondrocyte transplantation. *N Engl J Med* 331:889-895, 1994

[10]. Dashevsky JH: Arthroscopic measurement of chondromalacia of patella cartilage using a microminiature pressure transducer. *Arthroscopy*, 3:80-85, 1987

[11]. Frank EH, Grodzinsky AJ: Cartilage electromechanics-II. A continuum model of cartilage electrokinetics and correlation with experiments. *J Biomech*, 20:629-639, 1987

[12]. Geddes LA: *Electrodes and the Measurement of Bioelectric Events.* Wiley-Interscience, New York, 1972

[13]. Ghandilly FN, Thomas I, Orychak AF, Lalonde J-M: Long-term results of superficial defects in articular cartilage: a scanning electron microscope study. *J Pathol.* 121:213-217, 1977

[14]. Grodzinsky AJ, Kim YJ, Buschman, MD, Garcia AM, Quinn TM, Hunziker EB: Response of the chondrocyte to mechanical stimuli. In *Osteoarthritis.* Oxford University Press, Oxford, 1998

[15]. Grodzinsky, AJ. *Fields Force and Flows in Biological Tissues and Membranes.* Notes for MIT course 6.561, 1991.

[16]. Hardington TE, Fosang A: Proteoglycans: many forms and many functions. *FASEB* 6:861-870, 1992

[17]. Hoch DH, Grodzinsky AJ, Koob TJ, Albert ML, Eyre DR: Early changes if material properties of rabbit articular cartilage after meniscotomy. *J Orthop Res*, 1:4-12, 1983

[18]. Hochberg MC, McAlindon T, Felson DT: Systemic and topical treatments. In: Felson DT, conference chair. Osteoarthritis: new insights. Part 2: Treatment approaches. *Ann Intern Med.*133:726-729, 2000

[19]. Hunter, W: Of the structure and diseases of articulating cartilage. *Phil Trans.* 42:5114-21, 1743

[20]. Jordan JM, Kington RS, Lane NE, Nevitt MC, Zhang Y, Sowers MF, et al: Systemic risk factors of osteoarthritis. In: Felson DT, conference chair. Osteoarthritis: new insights. Part 1: The disease and its risk factors. *Ann Intern Med,* 133:637-639, 2000

[21]. Kang R, Ghivizzani SC, Muzzonigro TS, Herndon JH, Robbins PD, Evans CH: Orthopaedic Applications of Gene Therapy: From Concept to Clinic. *Clinical Orthopedics and Related Research,* 375:324-337, 2000

[22]. Kiefer GN, Sundby K, McAllister D, Shrive NG, Frank CB, Lam T, Schachar NS: The effect of cyropreservation on the biomechanical behavior of bovine articular cartilage. *J Orthop Res.* 7(4):494-501, 1989

[23]. Laupacis A, Bourne R, Rorabeck C, Feeny D, Wong C, Tugwell P, et al: Costs of elective total hip arthroplasty during the first year. Cemented vs noncemented. *J Arthroplasty*. 9:481-7, 1994

[24]. Lavernia, CJ, Guzman JF, Gachupin-Garcia A. Cost effectiveness and quality of life in knee arthroplasty. *Clin Orthop*, 345:134-9, 1997

[25]. Lee CR, Grodzinsky AJ, Hsu, H-P, Martin SD, Spector M: Harvest and selected cartilage repair procedures affect physical and biochemical properties of uninvolved articular cartilage in the canine knee. *JOR*, 18: 790-798, 2000

[26]. Lee CR: Physical *and Biochemical Properties of Canine Knee Articular Cartilage Are Affected by Selected Surgical Procedures.* Master's Thesis, Massachusetts Institute of Technology, 1999

[27]. Lee CR, Spector M: Status of articular cartilage tissue engineering. *Current Opinion in Orthopedics,* 9;VI:88-93, 1998

[28]. Levenston ME, Frank EH, Grodzinsky AJ: Electrokinetic and Poroelastic Coupling during Finite Deformations of Charged Porous Media. *Journal of Applied Mechanics*, Vol. 66 1-66, 1999

[29]. Lyrra T, Jurvelin J, Pitkanen P, Vaatainen U, Kiviranta I: Indention instrument for the measurement of cartilage stiffness under arthroscopic control. *Med Eng Phys*, 17:395-399, 1995

[30]. Malinin TI, Mnaymneh W, Lo HK, Hinkle DK: Cryopreservation of articular cartilage. Ultrastructural observations and long term results of experimental distal femoral transplantation. *Clin Orthop*, 303:18-32, 1994

[31]. Mankin HJ: The response of articular cartilage to mechanical injury. *J Bone Joint Surg Am*, 64:460-466, 1982

[32]. Minas T, Nehrer S: Current Concepts in the treatment of articular cartilage defects. *Orthopedics*, 20:525-538, 1997

[33]. Neuman MR: Biopotential Electrodes. In *Medical Instrumentation: Application and Design*. Houghton Mifflin Company, Boston, 1992.

[34]. Patwari P, Fay J, Cook M, Badger AM, Kerin AJ, Lark MW, Grodzinsky AJ. In Vitro Models for Investigation of the Effects of Acute Mechanical Injury on Cartilage. Submitted.

[35]. Poole CA: The structure and function of articular cartilage matrices. In JF Woessner, Jr and DS Howell, editors, *Joint Cartilage Degradation*, chapter 1, pages 1-35. Dekker, New York, 1993.

[36]. Quan EC, Treppo S, Butts E, Frank EH, Koepp H, Cole AA, Grodzinsky AJ: Detection of cartilage degradation in human patellae via tissue impedance measurements using a hand-held surface spectroscopy probe. *Trans ORS*, 1994.

[37]. Quan EC. *Design of an In-Vivo Probe to Detect Cartilage Degeneration.* Master's Thesis, Massachusetts Institute of Technology, Cambridge, MA, 1998

[38]. Radin EL, Pal IL. Response of joints to implant loading. 1. In vitro wear. *Arthritis Rheum*, 14:356-62, 1971

[39]. Rivers PA, Wang H, Strauch RJ, Athesian GA, Pawluk RJ, Rosenwasser MP, Ratcliffe A, Mow VC: Osteoarthritic changes in the biochemical composition of carpometacarpel joint cartilage and correlation with compressive modulus. *Trans Orthop Res Soc*, 23:754, 1998

[40]. Sachs JR, Grodzinsky AF: An electromechanically coupled poroelastic medium driven by an applied electric current: surface detection of bulk material properties. *Physiochem Hydrodyn*, 11:585-614, 1989.

[41]. Sachs JR: *A Mathematical Model of an Electromechanically Coupled Poroelastic Medium.* PhD Thesis, Massachusetts Institute of Technology, Cambridge, MA, 1987.

[42]. Salai M, Givon U, Messer Y, von Versen R: Electron microscopic study on the effects of different preservation methods for meniscal cartilage. *Ann Transplant,* 2(1):52-4, 1997

[43]. Salant, EP: *Surface Probe for Electrokinetic Detection of Cartilage Degeneration.* MD Thesis, Harvard-MIT Division of Health Sciences and Technology, Cambridge, MA, 1991

[44]. Sang QA, Douglas DA: Computational sequence analysis of matrix metalloproteinases. *J Pro Chem*, 15:137-160, 1996

[45]. Shapiro SD, Fliszar CJ, Broekelmann TJ, Mecham RP, Senior RM, Welgus HG: Activation of the 92-kd gelatinase by stromelysin and 4-aminophenyl mercuric acetate. Differential processing and stabilization of the carboxyl-terminal domain by tissue inhibitor of metalloproteinases (TIMP). *J Biol Chem*, 270:6351-6356, 1995

[46]. Shapiro F, Koide S, Glimcher MJ: Cell origin and differentiation in the repair of full-thickness defects of articular cartilage. *J Bone Joint Surg Am*, 75:532-552, 1993

[47]. Slemenda C, Brandt KD, Heilman DK, Mazzuca S, Braunstein EM, Katz BP, et al: Quadriceps weakness and osteoarthritis of the knee. *Ann Intern Med*, 127:97-104, 1997

[48]. Tavakol K, Miller RG, Bazett-Jones DP, Hwang WS, McGann LE, Schachar NS "Ultrastructural changes of articular cartilage chondrocytes associated with freeze-thawing" *J Orthop Res,* 11(1):1-9, 1993

[49]. Treppo S, Berkenblit SI, Bombard DL, Frank EH, Grodzinsky AF: Physical Diagnosis of Cartilage Degradation. In *Advances of Osteoarthritis,* pp 59-73. Springer-Verlag, Tokyo, 1999

[50]. Treppo, Steven: *Physical Diagnostics of Cartilage Degradation.* PhD Thesis, Harvard-MIT Division of Health Sciences and Technology, Cambridge, MA, 1999

[51]. University of Minnesota, Regents: Viscosupplementation for the Treatment of Osteoarthritis. 8 Dec. 2000. University of Minnesota Orthopaedics Sports Medicine Institute. 21 March 2001. http://www.sportsdoc.umn.edu/Patients%20Folder/Knee/Viscosupplementation.htm

[52]. Woessner JF Jr: Inhibition of matrix metalloproteinases: therapeutic potential. In *The Family of Matrix Metalloproteinases,* volume 732, pp. 11-21. The New York Academy of Sciences, New York, New York, 1994

[53]. Wood DJ, Awbrey BJ, Tomford WW, Butterfield L, Mankin HJ: Functional Results of Osteoarticular Allograft Reconstruction of the Knee. *American Academy of Orthopaedic Surgeons,* 1990.

[54]. Yacobucci G: Articular Cartilage Injury. Arthroscopic Surgery and Sports Medicine. 21 May 2001. YacoSportsMed. 21 May 2001. http://members.tripod.com/GeraldY/articularcartilageinjury.html, 2001.

[55]. Zaresky MC, Mouayad L, Melcher JR: Continuum properties from interdigitated electrode dieletrometry. *IEEE Trans Electr Insul*, 23:897-917, 1988